NutGEnIE 1.0: nutrient cycle extensions to the cGEnIE Earth system model to examine the long-term influence of nutrients on oceanic primary production

David A. Stappard[1], Jamie D. Wilson[2], Andrew Yool[3], Toby Tyrrell[1]

[1]School of Ocean and Earth Science, University of Southampton, Southampton, SO14 3ZH, United Kingdom
[2]Dept. of Earth, Ocean and Ecological Sciences, University of Liverpool, Liverpool, L69 3GP United Kingdom
[3]National Oceanography Centre, Southampton, SO14 3ZH, United Kingdom

Correspondence to: David A. Stappard (ds2n19@soton.ac.uk)

Abstract. Understanding the nuances of the effects of nutrient limitation on oceanic primary production has been the focus of many bioassay experiments by oceanographers. A theme of these investigations is that they identify the currently limiting nutrient at a given location, or in other words they identify the proximate limiting nutrient (PLN). However, the ultimate limiting nutrient (ULN; the nutrient whose supply controls system productivity over extensive timescales) can be different from the PLN. Our motivation is to investigate the identity of the ULN. The ULN constrains oceanic primary production over extensive timescales and consequently overall ocean fertility. The rate of oceanic photosynthesis affects planetary oxygen and carbon dioxide, impacting climate. Understanding past ocean fertility is fundamental to understanding Earth system history and biological evolution.

Investigations that have considered the ULN have often utilised box models for example the work of, Tyrrell (1999) and Lenton and Watson (2000). To facilitate this investigation of the ULN the **c**arbon-centric **G**rid **En**abled **I**ntegrated **E**arth system model (cGEnIE) **nut**rient cycles have been extended to create NutGEnIE. NutGEnIE incorporates three open nutrients cycles nitrogen, phosphorus, and iron. The impacts of diazotrophs, capable of fixing nitrogen, are represented alongside those of other phytoplankton. NutGEnIE is capable of extended duration model simulations necessary to investigate the ULN while, at the same time, including iron as a potentially limiting nutrient. NutGEnIE will beis described here, with particular focus on the biogeochemical cycles of iron, nitrogen and phosphorus. Model results are compared to ocean observational data to assess the degree of realism. Model-data comparisons include physical properties, nutrient concentrations, and process rates (e.g., export and nitrogen fixation). The comparisons of NutGEnIE to ocean observational data are largely positive, suggesting that the dynamics of NutGEnIE are valid. The validations, allied to the ability to run an Earth System model with open nutrients cycles of nitrogen, phosphorus, and iron over extensive time periods supports the proposed use of NutGEnIE to revisit the question of the ULN for oceanic primary production.

These comparisons support the conclusion that NutGEnIE is appropriate for the investigation of the ULN.

1 Introduction

1.1 The importance of oceanic primary production

Photosynthetic phytoplankton that inhabit the sunlit ocean surface, the euphotic zone, are responsible for the majority of ocean primary production (PP) and form the base of marine food webs. These photosynthetic phytoplankton, photoautotrophs, use light to fix dissolved carbon dioxide (CO_2) and other nutrients into biomass that fuels the pelagic ecosystem, and ultimately leads to the export of carbon to depth via a process known as the biological carbon pump (BCP) (Chisholm, 2000; Boyd et al., 2019). The strength of the BCP can influence atmospheric concentrations of CO_2 and therefore Earth's carbon cycle and climate (Sarmiento et al., 1998; Hain et al., 2014; Galbraith and Skinner, 2020). Net primary production (NPP) represents the~~is~~ total rate of organic carbon production minus the rate of respiration by phytoplankton; it therefore represents the rate that phytoplankton produce~~s~~ biomass (Sigman and Hain, 2012). Estimates of global marine NPP based on satellite, float or ecosystem models are ~ 50 - 60 petagrams of carbon per year (Pg C yr^{-1}) (Carr et al., 2006; Silsbe et al., 2016; Johnson and Bif, 2021). Ocean uptake of CO_2, mostly through abiotic processes, has contributed to mitigating much of the impact of anthropogenic CO_2 emissions with approximately half taken up by a combination of land and ocean carbon reservoirs (Ballantyne et al., 2012; Friedlingstein et al., 2022). Understanding of the controls on ocean NPP levels can provide insights into Earth's past, current and potential future carbon cycle. Nutrient supply to the euphotic zone acts as a fundamental control on ocean PP levels;~~,~~ this supply and subsequent growth limitation are the focus of the model extensions we present here.

1.2 Factors limiting primary production

Predation or grazing from higher trophic levels can be categorised as 'top-down' control of phytoplankton PP; by reducing phytoplankton populations, ~~grazing~~ consequently reduc~~es~~ing the total amount of photosynthesis. When not at optimal levels, light, temperature, and nutrients cause realised growth rates to be below the maximum growth rate of a phytoplankton population and can be considered as 'bottom-up' controls on PP. Light as a source of energy is an obvious potential limitation to photosynthetic phytoplankton. The nature of light limitation has been considered and methods of modelling it developed (e.g. Marra et al., 1985; Yang et al., 2020). Temperature also regulates biological rates as individual species have a relatively narrow optimal temperature range with growth declining rapidly outside this range (Gillooly et al., 2002). When community production is considered, growth rates ~~have an~~increase exponentia~~l~~ly ~~growth~~ with temperature as species with higher optimal growth ranges are favoured (Eppley, 1972); furthermore,~~ Again,~~ studies have proposed methods of modelling temperature limitation (e.g. Grimaud et al., 2017; O'Donnell et al., 2018).

Elements ~~(C, H, N, P, O and S)~~ obtained from nutrients are essential components of macro-molecules such as proteins and~~,~~ nucleic acids~~, etc.~~ (Moore et al., 2013). Nutrient limitation is a condition or state where addition of a nutrient would stimulate growth (Cullen, 1991; de Baar, 1994).~~ Nutrient stress refers to a physiological response to nutrient shortage (Cullen et al., 1992). Nutrient deficiency refers to the lack of one nutrient relative to others (Cullen, 1991). Nutrient co-limitation is a condition where the addition of multiple nutrients stimulates more growth than addition of any one nutrient alone (Arrigo, 2005; Saito et al., 2008) .~~ Addition of the proximate limiting nutrient (PLN)~~,~~ stimulates immediate growth, whereas addition of the ultimate limiting nutrient (ULN) enhances total system productivity over extensive timescales (Cullen, 1991; Tyrrell, 1999).

Much work has been conducted to describe the nature of phytoplankton nutrient requirements (Redfield, 1934, 1958) and subsequent limitation of growth (Sommer, 1986; Timmermans et al., 2004; Flynn, 2010; Bestion et al., 2018). Moore et al. (2013) and Browning and Moore (2023) conducted extensive analysis to compare nutrient availability to phytoplankton nutrient requirements. This work enabled the determination of spatial variations of proximate nutrient limitations. Further analysis linked nutrient deficiencies to large-scale ocean physical–chemical–biological processes (Moore, 2016).

Oceanographers have conducted numerous experiments to investigate nutrient limitation of oceanic PP. A great deal of this work has involved the use of bioassay experiments that consist of the addition of nutrients to samples of surface ocean water to determine which stimulates the greatest phytoplankton growth (Mills et al., 2004; Bonnet et al., 2008; Moore et al., 2008). The concept of iron fertilisation also gained focus following the work of Martin (1990), prompting a range of iron fertilisation experiments. These experiments involved in situ iron fertilisation (Martin et al., 1994; Boyd and Abraham, 2001; Hoffmann et al., 2006) - in effect field bioassay experiments. The implications of many bioassay and fertilisation experiments was summarised and synthesised by Moore et al. (2013), who were able to identify primary, secondary, and co-limiting nutrients across many regions. Moore (2016) compared the stoichiometry of the elemental requirements of phytoplankton to the elemental composition of ocean basins' deep water, that acts to supply nutrients to surface water. Browning and Moore (2023) conducted further synthesis of over 150 bioassay and fertilisation experiments, identifying three dominant nutrient limitation regimes. Their work suggest the ~~The~~ stratified subtropical gyres and summertime Arctic Ocean are nitrogen limited, upwelling regions are typically iron limited and remaining regions are most commonly co-limited by iron and nitrogen (Browning and Moore, 2023). The underlying bioassay experiments and analysis mentioned here have a common theme in that they focus on the immediate nutrient deficiency situation in a temporal sense, and often focus on a specific ocean location. This focus on the immediate nutrient deficiency identifies the PLN.

Tyrrell (1999) used a box model approach to identify nitrate as the PLN and phosphate as the ULN. In contrast, Falkowski (1997) argued that the dynamics of the nitrogen cycle, with particular emphasis on the limiting role iron has on nitrogen fixation, has ultimate control over phytoplankton productivity. Deutsch et al. (2007) concluded that nitrogen fixation stabilises the oceanic fixed nitrogen inventory over time but that water column denitrification rather than atmospheric inputs of iron determine nitrogen fixation rates. Moore and Doney (2007) concluded that for much of the global ocean iron is the ultimate limiting nutrient. There were some shortcomings in prior work to identify the ULN: (a) Tyrrell (1999) did not include iron, consequently the high iron requirements of the enzyme nitrogenase central to nitrogen fixation were not captured; (b) Falkowski (1997) provided an analysis based on the evolution of biogeochemical cycles, without supporting the analysis with modelling; (c) ~~The modelling of~~ Deutsch et al. (2007) ~~was~~ only conducted model simulations over short timescales to a modern ocean steady-state; and (d) Moore and Doney (2007) focused primarily on the nutrient regime of the Southern Ocean.

These shortcomings and other considerations suggest the desirability of a new modelling approach to the ULN question in which the model used possesses the following characteristics: (1) cycling and biological uptake of (and potential limitation by) all three nutrients (N, P, Fe), (2) nitrogen-fixing as well as non-fixing phytoplankton, (3) spatial resolution, as opposed, for instance, to representing the whole surface ocean with one box, (4) ~~but at the same time~~ the ability to carry out model runs exceeding the residence times of all three nutrients, and (5) external inputs (e.g. delivery of nutrients down rivers) and external outputs (e.g. delivery of nutrients to seafloor sediments via burial) in an 'open' model allowing total ocean inventories of nutrients to change over time

1.3 Investigating the Ultimate Limiting Nutrient

~~One way of modelling a system is to represent it by a mathematical model. The model abstraction can allow focus on features of interest. Models represent fundamental processes through a series of mathematical equations and parameterisations. Models provide insight into processes that are difficult or expensive to observe or even immeasurable. They give spatial and temporal coverage that would otherwise be unavailable. Through hypothesis testing, it is possible to examine *what if?* questions that would be impossible or undesirable to investigate in the real ocean. Models also allow an analysis of past events and insight into potential future scenarios that without a model would be unavailable.~~ Investigations that have considered ULN have often utilised box models for example the work of, Tyrrell (1999) and Lenton and Watson (2000).

Here we propose to establish a model approach that can be used subsequently to study the long-term influence of nutrients on PP and diagnose the ULN. Such investigations will require full ocean investigations to be executed over tens of thousands of

years, given the long residence times of nutrients in the global ocean. Delaney (1998) indicate phosphorus has a residence time of several tens of thousands of years, (phosphorus: several tens of thousands years (Delaney, 1998), nitrogen has a residence

115 time of : a few thousand years (Gruber, 2004) and iron a residence time of : tens to hundreds of years (Hayes et al., 2018)). For that to be successful the **c**arbon-centric **G**rid **En**abled **I**ntegrated **E**arth system model (cGEnIE), has been configured and modified to include the three open nutrient cycles fors nitrate, phosphate, and iron (Sect. 2) to create a variant referred to hereafter asa **nut**rient-centric **G**rid **En**abled **I**ntegrated **E**arth system model (NutGEnIE).

A background overview of the cNutGEnIE model framework is provided in Sect. 2.1 and 2.2, followed by a more detailed

120 descriptions of the critical aspects of NutGEnIE nutrient cycles that have been configured to support the ongoing analysis. Details of the validation approach (Sect. 3.1) and subsequent results (Sect. 3.2 to and 3.33.4) and discussion follow.

2 Model description

2.1 Physical model of cGEnIE

The ocean physics and climate model in cGEnIE are based on the fast climate model 'C-GOLDSTEIN' of Edwards and Marsh

125 (2005). C-GOLDSTEIN is comprised of a reduced physics (frictional geostrophic) 3-D ocean circulation model coupled to a 2-D energy–moisture balance model (EMBM) and a dynamic–thermodynamic sea ice model (Edwards and Marsh, 2005; Marsh et al., 2011). The ocean model calculates the horizontal and vertical transport of heat, salinity, and biogeochemical tracers using a parameterisation for isoneutral diffusion and eddy-induced advection (Edwards and Marsh, 2005; Marsh et al., 2011). The ocean model additionally determines heat and moisture exchanges with the atmosphere, sea ice, and land, and is

130 forced at the ocean surface by zonal and meridional wind stress according to a specified wind field. Horizontal transport of sea ice is resolved by the sea ice model in addition to the exchange of heat and fresh water with the ocean and atmosphere. A full description of the C-GOLDSTEIN model can be found in Edwards and Marsh (2005) and, with updates, in Marsh et al. (2011). The ocean model is configured on a 36x36 equal-area horizontal grid. The grid is uniform in longitude (10° increments) and uniform in the sine of latitude (resulting in latitude increments of approximately 3.2° at the Equator increasing to 19.2° at the

135 highest latitude). The ocean has 16 logarithmically spaced z-coordinate levels in the vertical. The thickness of the vertical levels increases with depth, from 80.8 m at the surface to 765 m at the deepest level. The configured representation of the grid and bathymetry is shown in Fig. 1. C-GOLDSTEIN is run with 96 time steps per year and is configured based on the parameterisation detailed in the fifth row (GENIE-16) of Table 1 of Cao et al. (2009).
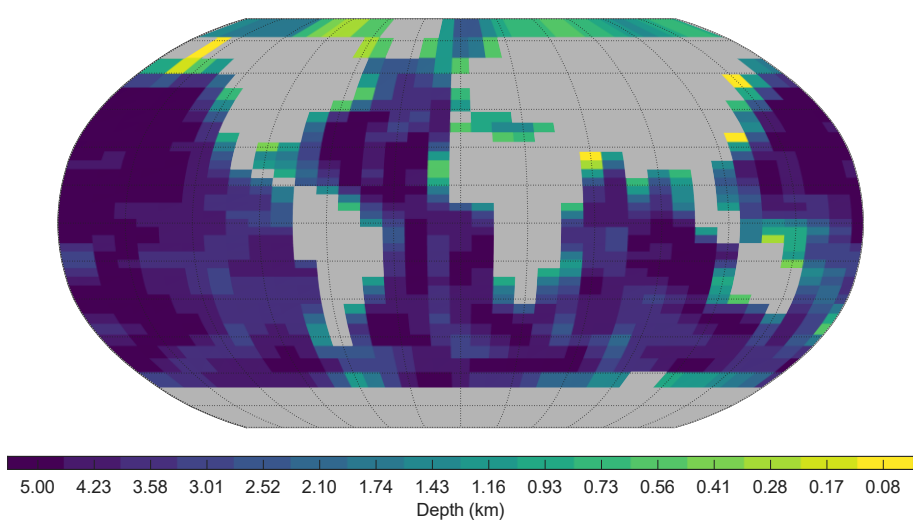

5.00 4.23 3.58 3.01 2.52 2.10 1.74 1.43 1.16 0.93 0.73 0.56 0.41 0.28 0.17 0.08
Depth (km)

140

Figure 1. The modern cGEnIE gridded continental configuration and ocean bathymetry (depth in km). Based on 16 depth levels and a 36 x 36 equal area grid of cGEnIE. Exact depths at the bottom of each depth level are provided in Table S1.

2.2 Biogeochemistry framework (BioGEM)

cGEnIE includes a series of geochemical tracers within the biogeochemical model component referred to as BIOGEM (Ridgwell et al., 2007). The biological part of BIOGEM is abstracted relative to reality and does not maintain explicit biomass tracers (such as phytoplankton concentrations) for ocean life (Ridgwell et al., 2007). Biological activity is estimated from surface nutrient uptake which in turn is immediately converted to particulate and dissolved organic matter (POM and DOM) in the surface ocean (Ridgwell et al., 2007). The subsequent processing associated with POM and DOM is discussed in detail in Sect. 2.3. This abstracted approach results in a computationally efficient model that represents biogenically-induced chemical fluxes (Maier-Reimer, 1993) and is capable of execution timescales required to investigate the ULN. The basis of the biological nutrient uptake and export scheme is similar to that of Parekh et al. (2005). This has in turn been developed subsequently by work of others including Monteiro et al. (2012) and Reinhard et al. (2020).

Three tracer categories (atmospheric, oceanic, and sedimentary) track biogeochemical processes within the cGEnIE model. Atmospheric tracers include carbon dioxide and oxygen. A more extensive range of ocean tracers is used: dissolved inorganic carbon (DIC) and dissolved oxygen; nitrate (NO_3^-) and ammonium (NH_4^+) as forms of fixed nitrogen or dissolved inorganic nitrogen (DIN); ~~the nutrient framework of fixed nitrogen or dissolved inorganic nitrogen (DIN = NO₃ + NH₄),~~ phosphate ~~(PO₄)~~(PO_4^-)~~, and~~; iron (Fe); dissolved organic matter, partitioned between carbon (DOC), nitrogen (DON), phosphorus (DOP), and iron (DOFe); tracers associated with the iron cycle to track ligands and complexed ligand-bound iron; and additional tracers that include dissolved dinitrogen (N_2), ~~N₂, ammonia,~~ calcium (Ca) and sulphate (SO_4^{2-}). Ocean tracers for POM are not used as POM is immediately remineralised following the scheme set out in Sect. ~~2.3.4~~ 2.3.7. Sedimentary tracers include POM (partitioned by nutrient), calcium carbonate and detrital material. By default, results are output as annual average~~s figures~~, however the BIOGEM module computes tracers at 48 time steps per year ~~giving~~ allowing the possibility of results ~~output~~ relating to shorter timeframes.

2.3 Biogeochemistry extensions (NutGEnIE)

The focus of this section is to describe the nutrient cycles and utilisation of those nutrients by PP~~.~~; a~~A~~ full list of ocean tracers enabled in the NutGEnIE configuration is provided in provided in Table S2. NutGEnIE is an extension to the BioGEM module within cGEnIE. The novel features of the configuration of NutGEnIE described here includes (a) the concurrent use of three open nutrient~~s~~ (N, P and Fe) cycles when determining phytoplankton growth (surface nutrient uptake) and (b) the representation of a second iron binding ligand class with stronger binding in the upper water column. The three nutrients N, P and Fe have been included in previous versions of cGEnIE (Monteiro et al., 2012; Naafs et al., 2019) but without the surface and seafloor input fluxes introduced here and with uniform ligand binding within the iron cycle. In this section we detail the most pertinent feature~~s~~ of BioGEM alongside the extensions made in NutGEnIE.

NutGEnIE does not maintain the biomass of phytoplankton or model grazing by zooplankton; it utilises the limiting nutrient concentration within cells to calculate the rate of creation of new phytoplankton. The nutrient uptake processes differ for the two classes of phytoplankton considered within the model. Diazotrophs (designated by the superscript Diaz) are those phytoplankton capable of nitrogen fixation. The other phytoplankton class (designated by the superscript OPhy) are not capable of nitrogen fixation and must source nitrogen from the DIN in the surface waters. Nutrient uptake by other phytoplankton (Γ^{OPhy}) is described in Sect. 2.3.1; similarly, nutrient uptake by diazotrophs (Γ^{Diaz}) is described in Sect. 2.3.2. The nutrient uptake terms (Γ^{OPhy} and Γ^{Diaz}) are calculated in the surface layer.

In NutGEnIE, nutrients taken up by phytoplankton are instantly converted to POM and DOM in the surface ocean. The ratio of POM to DOM is set by a configuration option calibrated against nutrient observations as described in Ridgwell et al. (2007). POM is subject to immediate gravitational sinking to the ocean interior, without lateral advection, where it is immediately remineralised. DOM (maintained as a tracer for each nutrient DOM_C, DOM_N, DOM_P and DOM_Fe) is subject to ocean

185   circulation_ and mostly retained in the surface ocean. DOM has an assumed lifetime governed by a degradation rate constant

(λ, 0.5 yr^{-1}) with remineralisation occurring as outlined in Sect. 2.3.7 ~~2.3.4~~ (Reinhard et al., 2020).

~~The nutrient uptake processes differ for the two classes of phytoplankton considered within the model. Diazotrophs (designated by the superscript Diaz) are those phytoplankton capable of nitrogen fixation. The other phytoplankton class (designated by the superscript OPhy) are not capable of nitrogen fixation and must source nitrogen from the DIN in the surface waters. Nutrient~~

190   ~~uptake by other phytoplankton (Γ^{OPhy}) is described in Sect. 2.3.2; similarly, nutrient uptake by diazotrophs (Γ^{Diaz}) is described in Sect. 2.3.3. The nutrient uptake terms (Γ^{OPhy} and Γ^{Diaz}) only have a value in the surface layer.~~

    We intend to use the model to investigate the ULN and for this purpose it is essential that nutrient cycles are open. Therefore, in NutGEnIE a removal (burial) flux is applied by removing a fixed proportion (k_{BF}) of nutrient uptake by other phytoplankton and diazotrophs from the modelled ocean. This represents a simplified instantaneous sediment burial term that is not coupled

195   to POM remineralisation dynamics. External inputs are also applied, via rivers and/or the atmosphere and seafloor. ~~The combined nutrient uptake by other phytoplankton and diazotrophs after the application of the burial removal flux is represented by Γ^{All} (Eq. (1)). Setting k_{BF} to a value of zero would negate this removal flux.~~

$$\Gamma^{All} = (1 - k_{BF})(\Gamma^{OPhy} + \Gamma^{Diaz}) \tag{1}$$

The portion of nutrient uptake; (Γ^{NOPhy} and Γ^{NDiaz} for other phytoplankton and diazotrophs respectively); that is available

200   for remineralisation is determined after the subtraction of the burial removal flux (k_{BF}), see Eq. (1 and 2). Within each surface cell a proportion (k_{BF}) of the nutrient uptake in that cell is lost and made unavailable for remineralisation. Setting k_{BF} to a value of zero would negate this removal flux mechanism. The values, units and brief description of equation constants are provided in Table 1.

$$\Gamma^{NOPhy} = (1 - k_{BF})\, \Gamma^{OPhy} \tag{1}$$

205
$$\Gamma^{NDiaz} = (1 - k_{BF})\, \Gamma^{Diaz} \tag{2}$$

    The understanding of the oceanic iron cycle has developed in recent years; a comprehensive summary is provided in Figure 2 of Tagliabue et al. (2017). Tagliabue et al. (2017) identify aeolian dust deposition, rivers, sea-ice, hydrothermal systems and sediments as sources of iron. The iron cycle of NutGEnIE has been extended so that it includes surface dust deposition, a surface flux that represents riverine inputs and a benthic flux to represent hydrothermal systems and sediments as sources of

210   iron.

    Nitrogen cycling within NutGEnIE represents the various forms of nitrogen; that is, nitrate, ammonium, dinitrogen, and organic nitrogen. The cycling is achieved by the processes of uptake of nitrate and ammonium by other phytoplankton, nitrogen fixation by diazotrophs, denitrification, and nitrification (Monteiro et al., 2012). However, in reality in oxygen minimum zones additional removal pathways exist, for instance dissimilatory nitrate reduction to ammonia and anaerobic ammonium oxidation

215   (anammox) (Lam et al., 2009). Like denitrification, ~~a~~Anammox converts DIN to ~~dinitrogen~~N_2, i.e. reducing the inventory of DIN (Lam et al., 2009). Because of their similar biogeochemical consequences, and because both only occur in low oxygen conditions, ~~It is therefore noted that~~ anammox is not represented ~~by the NutGEnIE~~as a separate ~~denitrification~~ process. Denitrification ~~that~~ is solely based on organic matter remineralisation.

    The structures of the phosphorus, ~~nitrate~~ DIN and iron cycles in NutGEnIE are shown in Fig. 2. Input and output fluxes

220   associated with each nutrient are shown alongside the primary processes that influence nutrient concentrations. Each nutrient cycle is discussed in more detail in the following sections. ~~,~~ ~~T~~the spatial distribution of input fluxes ~~(RP, RN, DDFe and BFe)~~surface PO_4^- (S_{PO_4} -), surface NO_3^- (S_{NO_3}), dust deposition of iron (DD_{Fe}) and seafloor flux of iron (B_{Fe}) are shown in Fig. S1 to S3.
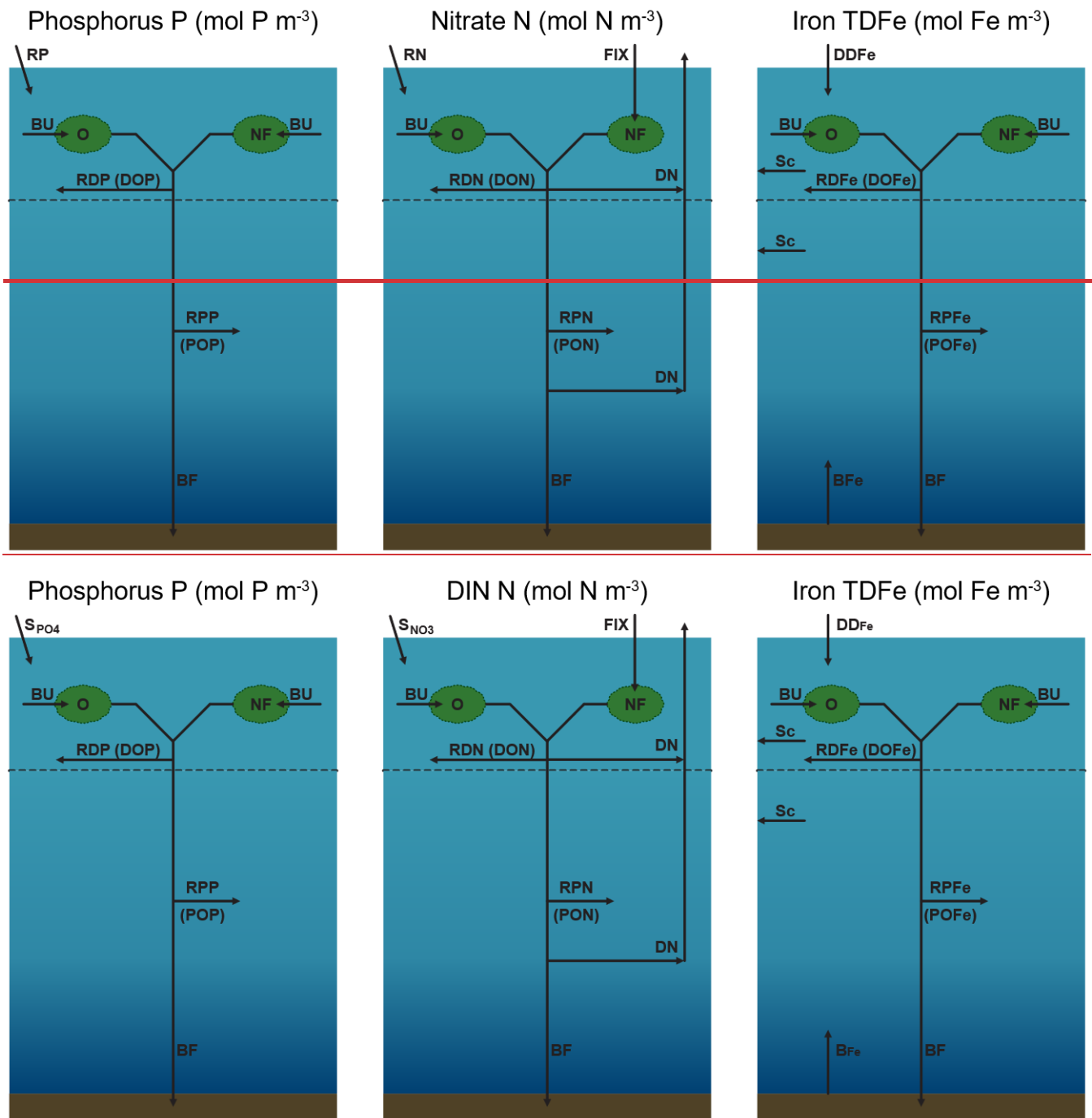
Figure 2. **Structure of NutGEnIE nutrient cycles.** DIN, dissolved inorganic nitrogen (DIN = $NO_3^- + NH_4^+$). TDFe, total dissolved iron. BU, biological uptake of nutrients by O, other phytoplankton and NF, nitrogen fixers (diazotrophs) occurs in the surface ocean layer. ~~River Surface~~ inputs (~~RP~~ S_{PO_4} and S_{NO_3} ~~RN~~) and dust deposition of iron (DDFe) are input fluxes to the surface ocean; BFe, ~~s~~Benthic (~~s~~eafloor) flux of iron; FIX, nitrogen fixation; DN, denitrification; Sc, scavenging of iron; BF, burial fraction; RDP, RDN and RDFe are remineralisation of dissolved organic phosphate (DOP), nitrate (DON) and iron (DOFe) respectively. RPP, RPN and RPFe are remineralisation of particulate organic phosphate (POP), nitrate (PON) and iron (POFe) respectively. Remineralisation of dissolved and particulate organic matter occurs throughout the water column.

2.3.1 Other phytoplankton nutrient uptake

Primary production (PP) is accounted for via the production of organic matter resulting from the uptake of nutrients. The nutrient framework is configurable, with an option to include silicon, but in NutGEnIE it is made to be dependent on DIN (= $NO_3^- + NH_4^+$), PO_4^- and Fe_T (= Fe' + FeL). Fe_T is the total bioavailable iron, which is discussed , along with the processes of iron complexation, in Sect. 2.3.6. Nutrient uptake by non-diazotrophs (other phytoplankton) results in the production of organic matter (Γ^{OPhy}) at a rate subject to Eq. (3) (Monteiro et al., 2012).

$$\Gamma^{OPhy} = V_{max}^{OPhy}(1-f_{ice})\gamma^T\gamma^I \, min\left[\frac{PO_4^-}{PO_4^-+K_P}; \frac{DIN}{DIN+K_N}; \frac{Fe_T}{Fe_T+K_{Fe}}\right] min\left[PO_4; \frac{DIN}{R_N^{OPhy}}; \frac{Fe_T}{R_{Fe}^{OPhy}}\right] \tag{3}$$

240 Nutrient limitation follows a Michaelis-Menten approach with a minimum law of nutrients. K_P, K_N, and K_{Fe} are the other phytoplankton half-saturation constants for phosphate, DIN, and iron, respectively. The concentration of the limiting nutrient therefore determines the other phytoplankton biomass, an approach that is often adopted in biogeochemical modelling (Maier-Reimer, 1993; Doney et al., 2006; Monteiro et al., 2012). V_{max}^{OPhy} is the maximum net nutrient uptake rate of other phytoplankton. The term $(1-f_{ice})$ ensures nutrient uptake is restricted to ice free locations as f_{ice} is the fraction of ice-

245 covered surface ocean. A temperature limitation term γ^T is based on an Eppley curve. $\gamma^T = Ae^{T/b}$, where T is the temperature (°C) and A and b the associated Eppley constants (Eppley, 1972; Bissinger et al., 2008). Light limitation is represented by γ^I, $\gamma^I = I/I_0$, where I is the amount of light and I_0 the solar constant (Monteiro et al., 2012). The uptake by other phytoplankton is in units of phosphorus. Therefore, DIN and Fe_T uptake are scaled by the other phytoplankton elemental composition ($R_N^{OPhy} = N{:}P$ and $R_{Fe}^{OPhy} = Fe_T{:}P$). The values, units and brief description of equation constants are provided in Table 2.

250 **2.3.2 Nitrogen fixation and diazotrophs nutrient uptake**

The activity of diazotrophs in NutGEnIE is also accounted for by the production of organic matter resulting from the uptake of nutrients. The availability of N_2 supplied via atmospheric transfer is deemed to be unlimited so that the production of organic matter (Γ^{Diaz}) is at a rate subject to Eq. (4) (Monteiro et al., 2012).

$$\Gamma^{Diaz} = V_{max}^{Diaz}(1-f_{ice})\gamma^T\gamma^I \, min\left[\frac{PO_4^-}{PO_4^-+K_P}; \frac{Fe_T}{Fe_T+K_{Fe}^{Diaz}}\right] min\left[PO_4^-; \frac{Fe_T}{R_{Fe}^{Diaz}}\right] \tag{4}$$

255 But this holds only if $\frac{DIN}{R_N^{OPhy}} < min\left[PO_4^-; \frac{Fe}{R_{Fe}^{OPhy}}\right]$ and $DIN < N_{thresh}$, otherwise the rate is zero. Together these two conditions only allow nitrogen fixation if DIN is scarce and if it is the limiting nutrient for other phytoplankton. V_{max}^{Diaz} is the maximum net nutrient uptake of diazotrophs and is assumed to be lower than V_{max}^{OPhy} because of the energy demands of the process of N_2 fixation. The ice fraction, temperature and light limitation aspects are the same as for other phytoplankton (Eq. (3) above). A higher Fe requirement for diazotrophs is consistent with the iron demands of the nitrogenase

260 enzyme (Berman-Frank et al., 2007). The values, units and brief description of equation constants are provided in Table 2. ~~(Monteiro et al., 2012)~~ Oligotrophic environments are defined as having $DIN < N_{thresh}$ (Monteiro et al., 2012). For the modern ocean a threshold can be constrained by observations leading to a fixed threshold $N_{thresh} \approx 2\ \mu mol\ DIN\ l^{-1}$ (Monteiro et al., 2011).

~~2.3.1~~2.3.3 Phosphorus ~~Nutrients and dissolved organic matter~~cycle and update

265 Here we cover the main governing equations in NutGEnIE. For each nutrient an equation is provided for it, alongside an equation for its dissolved organic matter, e.g., for phosphorus the equations for phosphate and DOP are provided. These equations represent the mechanism employed in NutGEnIE to maintain the tracer concentrations throughout the water column. Note that the transport terms calculated by the ocean circulation model (Edwards and Marsh, 2005) are omitted.

$$\frac{\partial \delta PO_4^- PO_4}{\partial \delta t} = -\Gamma_P^{OPhy} - \Gamma_P^{Diaz} + \lambda DOP + S_{PO_4} \tag{5\,2}$$

270 $$\frac{\partial \delta DOP}{\partial \delta t} = v(\Gamma_P^{AllNOPhy} + \Gamma_P^{NDiaz}) - \lambda DOP \tag{6\,3}$$

Γ_P^{OPhy} is the biological uptake of $PO_4^- PO_4$ by other phytoplankton as described in Sect. ~~2.3.2~~2.3.1. Similarly, Γ_P^{Diaz} is the biological uptake of $PO_4^- PO_4$ by diazotrophs ~~and is~~ described in Sect. 2.3.2~~2.3.3~~. A proportion (v) of the nutrients taken up by diazotrophs and other phytoplankton (Γ_P^{All}) is partitioned into DOM. This DOM is subsequently remineralised with a time constant (λ). The remaining proportion $(1-v)$ of the nutrient uptake is partitioned into POM that undergoes water column

275 remineralisation as detailed in Sect. 2.3.7~~2.3.4~~. The values of v and λ, are configurable, but in NutGEnIE are given default

values of $v = 0.66$ and $\lambda = 0.5\ yr^{-1}$ following the OCMIP-2 protocol (Najjar and Orr, 1999). The values, units and brief description of equation constants are provided in Table 1.

S_{PO_4} represents a surface input flux of PO_4 such as riverine inputs. The magnitude of this flux is configurable via a parameter that defines the annual moles of PO_4^- added. The S_{PO_4} flux is distributed evenly to cells adjacent to land (excluding Antarctica); all other cells, do not receive the input flux, see Fig. S1. The novel aspects of the phosphorus cycle in NutGEnIE are that it is open with a input flux S_{PO_4} and removal flux mechanism Eq. (1 and 2) allowing the phosphorus inventory to adjust. The input flux S_{PO_4} can be adjusted, as required for the future work to investigate the ULN.

2.3.4 Nitrogen cycle and update

Nutrient uptake by other phytoplankton is dependent on the availability of DIN, i.e., the combination of NO_3^- and NH_4^+ concentrations. The uptake rates of NO_3^- and NH_4^+ are represented by Eq. (7 and 8) with NH_4^+ being preferentially utilised (Naafs et al., 2019).

$$Up_{NH_4} = \min\ (\Gamma_N^{OPhy};\ NH_4^+) \tag{7}$$

$$Up_{NO_3} = \Gamma_N^{OPhy} - Up_{NH_4} \tag{8}$$

The governing equations for NH_4^+ and NO_3^- are below.

$$\frac{\partial NH_4^+}{\partial t} = -\ Up_{NH_4} - O_{Nit} + \lambda DON \tag{9}$$

$$\frac{\partial NO_3^-}{\partial t} = -\ Up_{NO_3} + O_{Nit} - R_{NO_3} + S_{NO_3} \tag{10}$$

$$\frac{\partial DON}{\partial t} = v(\Gamma_N^{NOPhy} + \Gamma_N^{NDiaz}) - \lambda DON \tag{11}$$

Nitrogen fixation is not explicitly represented in Eq. (9 to 11) but rather its impact is represented. Diazotroph organic matter (Γ_N^{Diaz}) is created without reducing concentrations of DIN, via nitrogen fixation, hence the Γ_N^{Diaz} term is not subtracted from nitrate or ammonium concentration in Eq. (9 and 10). However, all nutrient uptake ($\Gamma_N^{NOPhy} + \Gamma_N^{NDiaz}$) is added to the DON tracer concentration in Eq. (11) and ultimately available for remineralisation O_{Nit} represent the processes of nitrification, discussed immediately below. R_{NO_3} represent the denitrification process and is outlined in Sect. 2.3.7 and 2.3.4. The values, units and brief description of equation constants are provided in Table 1.

Nitrification is the process of oxidising ammonia to nitrate. The rate of nitrification (O_{Nit}) is determined by a two-substrate Michaelis-Menten formulation and allows for the limitation by both ammonium and oxygen (Naafs et al., 2019).

$$O_{Nit} = V_{max}^{Nit} \frac{O_2 \times NH_4^+}{\left(K_{O_2}^{Nit} \times K_{NH_4}^{Nit}\right) + \left(K_{O_2}^{Nit} \times NH_4^+\right) + \left(K_{NH_4}^{Nit} \times O_2\right) + (O_2 \times NH_4^+)}\ \min\left[NH_4^+, \frac{16}{138}O_2\right] \tag{12}$$

Where V_{max}^{Nit} is the maximum rate of nitrification, $K_{O_2}^{Nit}$ and $K_{NH_4}^{Nit}$ are the half-saturation constants for oxygen and ammonium (Naafs et al., 2019), the values, units and brief description of equation constants are provided in Table 4.

The novel aspects of the nitrogen cycle in NutGEnIE are the inclusion of an input flux S_{NO_3} and removal flux mechanism Eq. (1 and 2); the input flux S_{NO_3} can also be adjusted which will support the future work to investigate the ULN.

2.3.5 Iron cycle and uptake

NutGEnIE governing equations for Fe_T are below.

$$\frac{\partial Fe_T}{\partial t} = -\ \Gamma_{Fe}^{OPhy} - \Gamma_{Fe}^{Diaz} + \lambda DOFe + DD_{Fe} + B_{Fe} - k_{sc}Fe' \tag{13}$$

$$\frac{\partial DOFe}{\partial t} = v(\Gamma_{Fe}^{NOPhy} + \Gamma_{Fe}^{NDiaz}) - \lambda DOFe \tag{14}$$

9

The governing equation for iron contains an additional term, DD_{Fe}, that represents iron supplied via dust deposition. B_{Fe} represent an additional configurable input flux of iron applied to the seafloor layer. The prescribed dust deposition is achieved by a NutGEnIE forcing mechanism following a re-gridding from Mahowald et al. (2006), see Fig. S3. The processes associated with iron follow the methodology of Parekh et al. (2005). k_{sc} is a scavenging rate term that acts on free dissolved iron ~~III~~ (Fe′) throughout the water column. Honeyman et al. (1988) observed that particle concentration influences scavenging; its rate in NutGEnIE takes this into account by using a power law function to determine the scavenging rate:

$$k_{sc} = \tau k_0 (C_p)^\phi \qquad (15\cancel{8})$$

where k_0 is the scavenging rate (when particles are abundant), C_p is the particle concentration, and ϕ is a constant coefficient. The rate of scavenging is calculated as part of particle remineralisation which in turn is calculated as a function of the rate of creation of new particles in the upper ocean, which in turn is calculated from the nutrient uptake rate.

As Honeyman et al. (1988) empirically determined k_0 and ϕ using thorium, the scavenging rate is scaled by τ (Parekh et al., 2005). The values, units and brief description of equation constants are provided in Table 1. ~~The processes associated with ligand complexation are discussed in Sect. 2.3.7.~~ The novel aspects of the iron cycle in NutGEnIE are the inclusion of an input flux B_{Fe} and removal flux mechanism Eq. (1 and 2); the input fluxes DD_{Fe} and B_{Fe} can also be adjusted as is necessary to support the future work to investigate the ULN. Addition of a seafloor flux alongside the existing surface flux DD_{Fe} is a more realistic representation of ocean iron cycle fluxes (Tagliabue et al., 2017). The processes associated with ligand complexation have also been extended as discussed in Sect. 2.3.6.

2.3.2 Other phytoplankton nutrient uptake

~~NutGEnIE accounts for primary production (PP) via the production of organic matter resulting from the uptake of nutrients. The nutrient framework is configurable but here it is DIN (= NO₃ + NH₄), PO₄ and Fe. Nutrient uptake by non-diazotrophs (other phytoplankton) results in the production of organic matter (Γ^{OPhy}) at a rate subject to Eq. (9) (Monteiro et al., 2012).~~

$$\cancel{\Gamma^{OPhy} = V_{max}^{OPhy}(1 - f_{ice})\gamma^T \gamma^I \, min\left[\frac{PO_4}{PO_4 + K_P}; \frac{DIN}{DIN + K_N}; \frac{Fe}{Fe + K_{Fe}}\right] min\left[PO_4; \frac{DIN}{R_N^{OPhy}}; \frac{Fe}{R_{Fe}^{OPhy}}\right]} \qquad (9)$$

~~V_{max}^{OPhy} is the maximum net nutrient uptake rate of other phytoplankton. f_{ice} is the fraction of the surface ocean covered in ice. γ^T is a temperature limitation function based on an Eppley curve, $\gamma^T = Ae^{T/b}$, where T is the temperature (°C) and A and b the associated Eppley constants. γ^I is the light limitation function ($\gamma^I = I/I_0$, where I is the amount of light and I_0 the solar constant). Nutrient limitation follows Michaelis-Menten kinetics with a minimum law of nutrients. K_P, K_N, and K_{Fe} are the other phytoplankton half-saturation constants for phosphate, fixed nitrogen, and iron, respectively. The concentration of the limiting nutrient is used to determine the other phytoplankton biomass, as often assumed in biogeochemical modelling (Maier-Reimer, 1993; Doney et al., 2006; Monteiro et al., 2012). The uptake by other phytoplankton is in units of phosphorus. Therefore, DIN and Fe are scaled by the other phytoplankton elemental composition ($R_N^{OPhy} = N:P$ and $R_{Fe}^{OPhy} = Fe:P$).~~

2.3.6 Nitrogen fixation and diazotrophs nutrient uptake

~~The activity of diazotrophs in NutGEnIE is also accounted for by the production of organic matter resulting from the uptake of nutrients. The availability of dinitrogen (N₂) supplied via atmospheric transfer, is deemed to be unlimited so that the production of organic matter (Γ^{Diaz}) is at a rate subject to Eq. (10).~~

$$\cancel{\Gamma^{Diaz} = V_{max}^{Diaz}(1 - f_{ice})\gamma^T \gamma^I \, min\left[\frac{PO_4}{PO_4 + K_P}; \frac{Fe}{Fe + K_{Fe}^{Diaz}}\right] min\left[PO_4; \frac{Fe}{R_{Fe}^{Diaz}}\right]} \qquad (10)$$

~~But only if $\frac{DIN}{R_N^{OPhy}} < min\left[PO_4; \frac{Fe}{R_{Fe}^{OPhy}}\right]$ and $DIN < N_{thresh}$, otherwise the rate is zero. Together these two conditions only allow nitrogen fixation if DIN is scarce and it is the limiting nutrient for other phytoplankton.~~

V_{max}^{Diaz} is the maximum net nutrient uptake of diazotrophs and is assumed to be lower than V_{max}^{OPhy} because of the energy demands of the process of N_2 fixation. The ice fraction, temperature and light limitation aspects are the same as for other phytoplankton (Eq. (9) above). A higher Fe requirement for diazotrophs is consistent with the iron demands of the nitrogenase enzyme (Berman-Frank et al., 2007).

The conditions associated with Eq. (10) restrict nitrogen fixation to occurring in oligotrophic environments where DIN is the most limiting nutrient (defined as $DIN/R_N^{OPhy} < \min[PO_4; Fe/R_{Fe}^{OPhy}]$ for other phytoplankton). Oligotrophic environments are defined as having $DIN < N_{thresh}$ with N_{thresh} discussed in Sect. 2.3.5.

The computations associated with Eq. (9 and 10) are executed each time step, that is, 48 times per year. The values of V_{max}^{OPhy} and V_{max}^{Diaz} are 16 yr^{-1} and 0.7 yr^{-1} respectively; the maximum computed values of the associated limiting terms γ^T, γ^I, $\min\left[\frac{PO_4}{PO_4+K_P}; \frac{DIN}{DIN+K_N}; \frac{Fe}{Fe+K_{Fe}}\right]$, and $\min\left[\frac{PO_4}{PO_4+K_P}; \frac{Fe}{Fe+K_{Fe}^{Diaz}}\right]$ are 4.3, 0.8, 0.7, and 0.5 respectively. Therefore, the maximum percentage of the grid cell nutrient concentration taken up by other phytoplankton each time step is 80% (2.5% by diazotrophs).

2.3.13 Organic matter (OM) remineralisation

OM is split into two fractions, labile and refractory (refrac). OM is remineralised through the water column according to Eq. (11), an exponential function of depth (Monteiro and Ridgwell, 2023).

$$F^{POM}(z) = F^{POM}(z=z_0)\left(r_{labile}^{POM}e^{\left[\frac{z_0-z}{l_{labile}}\right]} + (1-r_{labile}^{POM})e^{\left[\frac{z_0-z}{l_{refrac}}\right]}\right) \tag{11}$$

$F^{POM}(z)$ is the POM flux at depth z. z_0 is the depth of the base of the photic zone. The labile fraction of POM is r_{labile}^{POM}, consequently, the refractory fraction of POM is $(1-r_{labile}^{POM})$. l_{labile} and l_{refrac} are the e-folding depths of remineralisation for labile POM and refractory POM.

OM decomposition is partitioned via a series of redox reactions: initially aerobic respiration utilising O_2 as the electron acceptor, secondly denitrification utilising NO_3 as the electron acceptor, and lastly sulfate reduction utilising SO_4 as the electron acceptor. Electron acceptors (O_2, NO_3, and SO_4) are consumed according to decreasing free energy yields (Froelich et al., 1979). Consumption rates of electron acceptors in the process of OM remineralisation follow Eq. (12 to 14) and take account of both electron acceptors abundance and the inhibitory effect of electron acceptors with higher free energy yield (Reinhard et al., 2020). Equation (12) can be considered to represent aerobic respiration, Eq. (13) represents nitrate reduction / denitrification, and Eq. (14) represents sulfate reduction.

$$R_{O_2} = \frac{[O_2]}{K_{O_2}+[O_2]} \tag{12}$$

$$R_{NO_3} = \frac{[NO_3]}{K_{NO_3}+[NO_3]}\frac{K_{O_2}^i}{K_{O_2}^i+[O_2]} \tag{13}$$

$$R_{SO_4} = \frac{[SO_4^-]}{K_{SO_4^-}+[SO_4^-]}\frac{K_{O_2}^i}{K_{O_2}^i+[O_2]}\frac{K_{NO_3}^i}{K_{NO_3}^i+[NO_3]} \tag{14}$$

where R_t indicates the relative fraction of each electron acceptor consumed, K_t are the half-saturation constants for each redox reaction and K_t^i are the inhibition constants to reduce redox reactions of lower yielding free energy. Redfield stoichiometry defines the elemental ratios of OM (C:N:P = 106:16:1) with the following redox pathways (Froelich et al., 1979).

$$(CH_2O)_{106}(NH_3)_{16}(H_3PO_4) + 138O_2 \rightarrow 106CO_2 + 16HNO_3 + H_3PO_4 + 122H_2O \tag{15}$$
$$\Delta G° = -3190 \, KJ \, mol^{-1}$$
$$(CH_2O)_{106}(NH_3)_{16}(H_3PO_4) + 94.4HNO_3 \rightarrow 106CO_2 + 55.2N_2 + H_3PO_4 + 177.2H_2O \tag{16}$$
$$\Delta G° = -3030 \, KJ \, mol^{-1}$$
$$(CH_2O)_{106}(NH_3)_{16}(H_3PO_4) + 53SO_4^{2-} \rightarrow 106CO_2 + 16NH_3 + 53S^{2-} + H_3PO_4 + 106H_2O \tag{17}$$

2.3.36 2.3.6 Ligand scheme enhancement in NutGEnIE

The iron cycle involves two processes that act on Fe' that are not like other cycles, scavenging and complexation. Fe' can be scavenged and is lost as particulate iron, which is thereafter is not available for biological uptake. Secondly, Fe' can be complexed with a free ligand (L') to form complexed iron (FeL). Complexed iron can in turn disassociate, reverting to free iron and a free ligand. An equilibrium is established so that Fe' + L' ⇌ FeL. Both Fe' and FeL are available for biological uptake. Scavenging, complexation, and biological uptake processes are shown in Fig. 3. Total iron (Fe_T) is the sum of free and complexed iron $Fe_T = Fe' + FeL$. Total ligand (L_T) is the sum of free and complexed ligands $L_T = L' + FeL$. It is Fe_T and L_T that are maintained as tracers with L_T having a fixed inventory, Table S2.

Complexation of Fe' and L' to FeL occurs on the timescales of minutes to hours (Witter et al., 2000) such that it is valid to assume that the complexation reaction goes to equilibrium. An equilibrium relationship constant (k_{FeL}), where k_{FeL} = [FeL]/[Fe'][L'], can be used to determine the speciation of iron (Parekh et al., 2004). A ligand strength, or stability constant, ($\log(k_{FeL}) = 11.0$) is used which is based on field and laboratory studies and sensitivity analysis (Parekh et al., 2004). Higher values of the stability constant, $\log(k_{FeL})$, imply a stronger binding ligand, and lower values a weaker binding ligand. The ligand scheme described above is based on the work of Archer and Johnson (2000), Parekh et al. (2004) and Parekh et al. (2005)
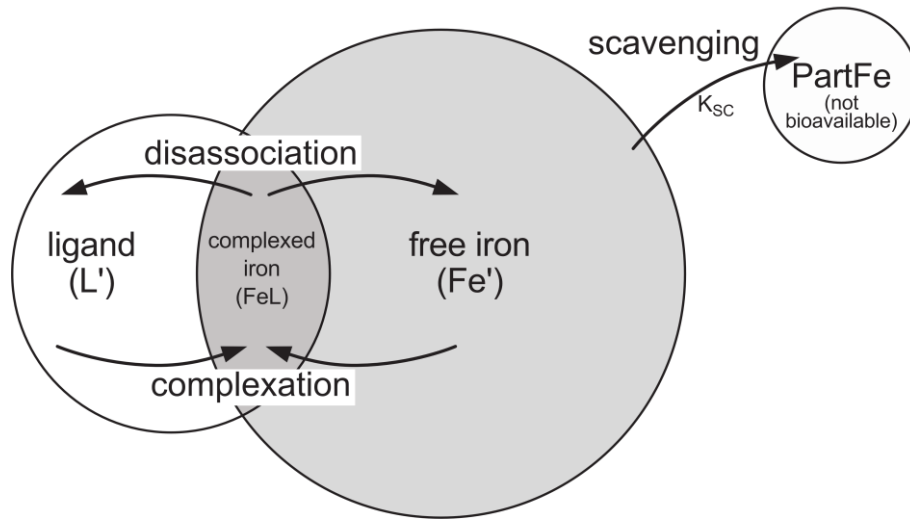
~~Complexation of Fe' and L' to FeL occurs on the timescales of minutes to hours (Witter et al., 2000) such that it is valid to assume that the complexation reaction goes to equilibrium. An equilibrium relationship constant (k_{FeL}), where $k_{FeL} =$~~
425 ~~[FeL]/[Fe'][L'], can be used to determine the speciation of iron (Parekh et al., 2004). A ligand strength, or stability constant, (log (k_{FeL}) = 11.0) is used which is based on field and laboratory studies and sensitivity analysis (Parekh et al., 2004). Higher values of the stability constant, log (k_{FeL}), imply a stronger binding ligand, and lower values a weaker binding ligand. The ligand scheme described above is based on the work of Archer and Johnson (2000), Parekh et al. (2004) and Parekh et al. (2005)~~

430 However, ~~R~~research has indicated differing ligand classes with differing binding strengths as well as a varying distribution of ligands through the water column. Schemes with dual ligand classes have been proposed with a strong binging ligand L_1 in surface waters and a moderate binding class L_2 throughout the water column (Hunter and Boyd, 2007; Ye et al., 2009; Misumi et al., 2013; Völker and Tagliabue, 2015). Differing distributions of L_1 and L_2 are of interest when considering global modelling (Misumi et al., 2013; Völker and Tagliabue, 2015; Boyd and Tagliabue, 2015; Ye et al., 2020). The behaviour of ligand class
435 L_2 is analogous with the single ligand class scheme described above (Parekh et al., 2005). The net effect of schemes with dual ligand classes is to have strong binging ligands at the surface. This stronger binging surface ligand behaviour has been addressed by creating a dynamic stability constant that can be configured for each NutGEnIE depth level.

The binding characteristics of ligands are~~is~~ represented by a stability constant (k_{FeL}) which, in NutGEnIE, has been made configurable independently for each depth level ~~rather than homogeneous which would dictate a uniform ligand binding~~
440 ~~scheme~~. A default value of k_{FeL} is configured with the ability to override this at each depth level by providing a depth level specific stability constant k_{FeL}^n, where n ~~has a value of~~denotes the layer, from 16 (surface layer) to 1 (deepest layer). The existence of a strong binging ligand class predominantly present in the upper water column is represented by setting a higher value of k_{FeL}^{16} (log (k_{FeL}^{16}) = 11.4) in the surface layer of NutGEnIE. For all other layers the value is the default value.

2.3.7 Organic matter (OM) remineralisation

445 OM is split into two fractions, labile and refractory (refrac). OM is remineralised through the water column according to Eq. (16), an exponential function of depth (Reinhard et al., 2020).

$$F^{POM}(z) = F^{POM}(z = z_0)\left(r_{labile}^{POM}e^{\left[\frac{z_0-z}{l_{labile}}\right]} + (1 - r_{labile}^{POM})e^{\left[\frac{z_0-z}{l_{refrac}}\right]}\right) \tag{16}$$

$F^{POM}(z)$ is the POM flux at depth z. z_0 is the depth of the base of the photic zone. The labile fraction of POM is r_{labile}^{POM}; consequently, the refractory fraction of POM is $(1 - r_{labile}^{POM})$. l_{labile} and l_{refrac} are the e-folding depths of remineralisation for labile POM and refractory POM. The values, units and brief description of equation constants are provided in Table 7.

OM decomposition is partitioned via a series of redox reactions: initially aerobic respiration utilising O_2 as the electron acceptor, secondly denitrification utilising NO_3^- as the electron acceptor, and lastly sulfate reduction utilising SO_4^{2-} as the electron acceptor. Electron acceptors (O_2, NO_3^-, and SO_4^{2-}) are consumed according to decreasing free energy yields (Froelich et al., 1979). Consumption rates of electron acceptors in the process of OM remineralisation are relative to R_i in Eq. (17 to 19) and take account of both electron acceptors abundance and the inhibitory effect of electron acceptors with higher free energy yield (Reinhard et al., 2020). Equation (20) can be considered to represent aerobic respiration, Eq. (21) represents nitrate reduction / denitrification, and Eq. (22) represents sulfate reduction.
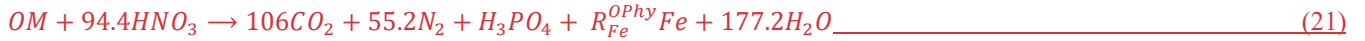
$$R_{O_2} = \frac{[O_2]}{K_{O_2} + [O_2]} \tag{17}$$

$$R_{NO_3} = \frac{[NO_3^-]}{K_{NO_3} + [NO_3^-]} \frac{K_{O_2}^i}{K_{O_2}^i + [O_2]} \tag{18}$$

$$R_{SO_4} = \frac{[SO_4^{2-}]}{K_{SO_4} + [SO_4^{2-}]} \frac{K_{O_2}^i}{K_{O_2}^i + [O_2]} \frac{K_{NO_3}^i}{K_{NO_3}^i + [NO_3^-]} \tag{19}$$

where R_i indicates the relative fraction of each electron acceptor consumed, K_i are the half-saturation constants for each redox reaction and K_i^i are the inhibition constants to reduce redox reactions of lower free energy yields. The values, units and brief description of equation constants are provided in Table 7.

Redfield stoichiometry defines the primary elemental ratios of OM; in addition, OM contains Fe determined by the parameter R_{Fe}^{OPhy}, see Table 2, resulting in elemental ratios of C:N:P:Fe = 106:16:1:R_{Fe}^{OPhy}. The remineralisation process follows the redox pathways of Eq. (20 to 22) (Froelich et al., 1979).

$$OM + 138O_2 \rightarrow 106CO_2 + 16NH_4 + H_3PO_4 + R_{Fe}^{OPhy}Fe + 122H_2O \tag{20}$$

$$OM + 94.4HNO_3 \rightarrow 106CO_2 + 55.2N_2 + H_3PO_4 + R_{Fe}^{OPhy}Fe + 177.2H_2O \tag{21}$$

$$OM + 53SO_4^{2-} \rightarrow 106CO_2 + 16NH_4 + 53S^{2-} + H_3PO_4 + R_{Fe}^{OPhy}Fe + 106H_2O \tag{22}$$

OM decomposition when oxygen levels are low leads to the use of nitrate as an alternative electron acceptor. Therefore, Eq. (21) above represents denitrification in NutGEnIE.

2.3.38 2.3.8 NutGEnIE configuration parameters

The NutGEnIE model has an implicit ecosystem and therefore appropriate values for constants are not immediately apparent from observations or experimental outputs. The constants associated with the processes set out in sections above are based on previous calibrations of cGEnIE (Ridgwell et al., 2007; Monteiro et al., 2012; Reinhard et al., 2020; van de Velde et al., 2021) with adjustments associated with the three open nutrient cycle configuration. The parameters associated with nutrient tracers, nutrient uptake, remineralisation, nitrification, and iron cycle are outlined in Tables 1 to 5. Monteiro and Ridgwell (2023) carried out significant work in the addition of the nitrogen cycle to cGEnIE; parameter values used in their work were the initial values used for the NutGEnIE configuration. The atmosphere of NutGEnIE is set to and maintained at a pre-industrial CO_2 concentration of 278 part per million (ppm).

In many cases parameters, particularly those associated with nutrient uptake, have been determined as the result of a calibration or tuning exercise. Parameters were adjusted to result in a combination that showed best agreement with observed nutrient distributions the concentrations of nutrients, the scale of pertinent processes (e.g., export and nitrogen fixation), and the spatial variations of nutrient uptake limitations. The determination of the best parameter combination used the techniques outlined in Sect. 3 information relating to the tuning exercise is provided in Sect 1.3 in supplementary materials.

Table 1 Biogeochemical parameters of NutGEnIE relating to nutrient tracers. These parameters relate to Eq (1~~-~~2, 5-11, 13-15~~to 8~~). Where the model value of the parameter differs from the literature reference value, the literature value is provided.

Name	Model value	Unit	Description and literature reference
k_{BF}	0.0048	-	Burial fraction, 0.0016 (Schlesinger, 1991).
λ	0.5	yr^{-1}	Remineralised time constant (Najjar and Orr, 1999).
v	0.66	-	DOM Partition (Najjar and Orr, 1999).
$1-v$	0.34	-	POM Partition.
k_0	0.079	d^{-1}	Initial iron scavenging rate (Honeyman et al., 1988).
ϕ	0.58	-	Exponent coefficient of iron scavenging (Honeyman et al., 1988).
τ	0.505	-	Iron sScavenging scaling factor, 0.2 (Parekh et al., 2005).

490

k_{BF}	0.0048	-	Burial fraction, 0.0016 (Schlesinger, 1991).
λ	0.5	yr^{-1}	Remineralised time constant (Najjar and Orr, 1999).

Table 2 Biogeochemical parameters of NutGEnIE relating to nutrient uptake. These parameters relate to Eq. (39 and 410). Where the model value of the parameter differs from the literature reference value, the literature value is provided.

Name	Model value	Unit	Description and literature reference
V_{max}^{OPhy}	16	yr^{-1}	Maximum net nutrient uptake (removal) rate by other phytoplankton.
A	0.59	-	First temperature-dependent uptake rate modifier (Bissinger et al., 2008).
b	15.8	-	Second temperature-dependent uptake rate modifier (Bissinger et al., 2008).
I_0	1,368	$W\ m^{-2}$	Solar constant (light).
K_P	0.14	$\mu mol\ P\ kg^{-1}$	Phosphate half-saturation constant.
K_N	3.3	$\mu mol\ N\ kg^{-1}$	Nitrate half-saturation constant.
K_{Fe}	0.27	$nmol\ Fe\ kg^{-1}$	Iron half-saturation constant.
R_N^{OPhy}	16	-	Other phytoplankton N:P elemental ratio (Redfield, 1934, 1958).
R_{Fe}^{OPhy}	1.93 x 10^{-3}	-	Other phytoplankton Fe:P elemental ratio. Determined from K_{Fe} / K_P.
V_{max}^{Diaz}	0.67	yr^{-1}	Maximum net nutrient uptake (removal) rate by diazotrophs
K_{Fe}^{Diaz}	0.54	$nmol\ Fe\ kg^{-1}$	Iron half-saturation constant for diazotrophs.
R_{Fe}^{Diaz}	3.86 x 10^{-3}	-	Diazotrophs Fe:P elemental ratio. Determined from K_{Fe}^{Diaz} / K_P.

Table 3 Nutrient cycle fluxes applied to NutGEnIE. These parameters relate to Eq (5, 10 and 13).

Name	Model value	Unit	Description and literature reference
S_{PO_4}	7.3 x 10^{10}	$mol\ P\ yr^{-1}$	Surface input flux of phosphate (Benitez-Nelson, 2000).
S_{NO_3}	3.2 x 10^{12}	$mol\ N\ yr^{-1}$	Surface input flux of nitrate (Gruber and Sarmiento, 1997; Gruber, 2008).
DD_{Fe}	8.4 x 10^8	$mol\ Fe\ yr^{-1}$	Surface dust deposition flux of iron (Fung et al., 2000; Luo et al., 2005; Moore and Braucher, 2008; Moore et al., 2008).
DDB_{Fe} ~~τ~~	8.0 x 10^8 ~~7.3 x 10^{10}~~	$mol\ Fe$ ~~N~~ yr^{-1} ~~-~~	Seafloor input flux of iron (Moore and Braucher, 2008; Tagliabue et al., 2010). ~~Surface input flux of phosphate~~

Table 4 Biogeochemical parameters of NutGEnIE relating to Nitrification. The parameters relate to Eq. (12).

Name	Model value	Unit	Description and literature reference
V_{max}^{Nit}	7.3	yr^{-1}	Nitrification maximum constant rate.
$K_{O_2}^{Nit}$	0.02	$\mu mol\ kg^{-1}$	Nitrification half-saturation constant for oxygen (Naafs et al., 2019).
$K_{NH_4}^{Nit}$	0.01	$\mu mol\ kg^{-1}$	Nitrification half-saturation constant for ammonium (Naafs et al., 2019).

Table 5 Biogeochemical parameters of NutGEnIE relating to the iron cycle. The parameters relate to the text of Sect. 2.3.6.

Name	Model value	Unit	Description and literature reference
$\log(k_{FeL})$	11	-	Default log of association constant for ligands (Parekh et al., 2004).
$\log(k_{FeL}^{16})$	11.4	-	Log of association constant for ligands in surface waters (Parekh et al., 2004).

495

500

Table $\underline{6}\cancel{3}$ Biogeochemical parameters of NutGEnIE relating to remineralisation. These parameters relate to Eq. (~~11~~ 16 to ~~1~~22 4). Where the model value of the parameter differs from the literature reference value, the literature value is provided.

Name	Model value	Unit	Description and literature reference
r_{labile}^{POM}	0.945	-	Labile fraction of POM (Reinhard et al., 2020).
r_{refrac}^{POM}	0.055	-	Refractory fraction of POM (Reinhard et al., 2020).
l_{labile}	590	m	e-folding depth of remineralisation for labile POM (Reinhard et al., 2020).
l_{refrac}	10^6	m	e-folding depth of remineralisation for refractory POM (Reinhard et al., 2020).
K_{O_2}	29.16	$\mu mol\ kg^{-1}$	half-saturation constant for aerobic respiration ~~(Monteiro and Ridgwell, 2023)~~.
$K_{O_2}^i$	4.50	$\mu mol\ kg^{-1}$	inhibition constant for aerobic respiration ~~(Monteiro and Ridgwell, 2023)~~.
K_{NO_3}	81.54	$\mu mol\ kg^{-1}$	half-saturation constant for nitrate reduction (denitrification) ~~(Monteiro and Ridgwell, 2023)~~.
$K_{NO_3}^i$	81.54	$\mu mol\ kg^{-1}$	inhibition constant for nitrate reduction (denitrification) ~~(Monteiro and Ridgwell, 2023)~~.
K_{SO_4}	500	$\mu mol\ kg^{-1}$	half-saturation constant for sulfate reduction (Olson et al., 2016).
$K_{SO_4}^i$	1000	$\mu mol\ kg^{-1}$	inhibition constant for sulfate reduction (Olson et al., 2016).

505 ~~Table 4 Biogeochemical parameters of NutGEnIE relating to Nitrification. The parameters relate to Eq. (18).~~

~~Name~~	~~Model value~~	~~Unit~~	~~Description and literature reference~~
~~V_{max}^{Nit}~~	~~7.3~~	~~yr^{-1}~~	~~Nitrification maximum constant rate (Monteiro and Ridgwell, 2023).~~
~~$K_{O_2}^{Nit}$~~	~~0.02~~	~~$\mu mol\ kg^{-1}$~~	~~Nitrification half-saturation constant for oxygen (Monteiro and Ridgwell, 2023).~~
~~$K_{NH_4}^{Nit}$~~	~~0.01~~	~~$\mu mol\ kg^{-1}$~~	~~Nitrification half-saturation constant for ammonium (Monteiro and Ridgwell, 2023)~~

~~Table 5 Biogeochemical parameters of NutGEnIE relating to the iron cycle. The parameters relate to the text of Sect. 2.3.7.~~

~~Name~~	~~Model value~~	~~Unit~~	~~Description and literature reference~~
~~$log(k_{FeL}^-)$~~	~~11~~	~~–~~	~~Default log of association constant for ligands.~~
~~$log(k_{FeL}^{16})$~~	~~11.4~~	~~–~~	~~Log of association constant related to ligands in surface waters.~~

~~4~~2 3 Model validation results

The cGEnIE model has been used extensively, with many studies examining the validity of the cGEnIE approach and

510 experiment results (Ridgwell et al., 2007; Monteiro et al., 2012; Tagliabue et al., 2016; Reinhard et al., 2020; van de Velde et al., 2021). A complete validation analysis of cGEnIE and its capabilities of representing the ocean and its processes is not undertaken here. The aim in the validation in this paper is to asses the pertinent biogeochemical distributions and processes that are relevant to the proposed use of NutGEnIE. NutGEnIE will be used to consider the effect nutrient supply has on PP and this informs the biogeochemical processes considered in the validation process. Nutrient concentrations and distributions are

515 evaluated because they influence PP which is central to the intended purpose (identification of the ULN). The processes of photosynthesis, respiration and remineralisation occur at differing depths of the ocean water column and each exert an influence on the concentration of dissolved oxygen. The concentration of dissolved oxygen is therefore a useful indicator of biogeochemical processes and, hence, also worthy of evaluation here. In Sect. 2.2 above, the concept that NutGEnIE represents PP by nutrient uptake and the subsequent formation or organic matter was discussed. In NutGEnIE a proportion of this organic

520 matter sinks from the ocean surface and therefore POC export is also compared to observations.

42.13.1 Datasets and methods

The World Ocean Atlas (WOA) 2018 provides annual climatology data based on observed ocean properties that are utilised for comparison purposes. These properties include temperature (Locarnini et al., 2018), salinity (Zweng et al., 2018), phosphate concentrations (Garcia et al., 2018a), nitrate concentrations (Garcia et al., 2018a) and dissolved oxygen concentrations (Garcia et al., 2018b). The WOA datasets are provided with a spatial resolution of 1° x 1° grid and 102 depth levels from surface to 5 500 m.

The GEOTRACES Intermediate Data Product 2021 dataset contains data from cruises measuring multiple hydrographic parameters, trace metals, and isotopes (GEOTRACES Intermediate Data Product Group, 2021; GEOTRACERS, 2022) (Schlitzer, 2014). GEOTRACES provides depth profiles of ocean dissolved iron concentration measurements in the Atlantic, Pacific and Southern Oceans that were compared to NutGEnIE concentrations using depth profiles. Cruises GA02 (Mar 2011 – Apr 2011) and GIPY05 (Feb 2008 – Apr 2008) covered the Atlantic Ocean and Southern Ocean respectively while GPc06 (Aug 2005 – Sep 2005) and GP19 (Dec 2014 – Feb 2015) provided coverage of the Pacific Ocean.

The Oregon State University Ocean Productivity group (Ocean Productivity, 2024) provide computations, based on observational data, of vertically integrated net PP (NPP). Differing methodologies for the computation of NPP are supported by the Ocean Productivity group. The observational rate of NPP (g C m^{-2} d^{-1}) used for comparison purposes here is the mean of values from the VGPM (Behrenfeld and Falkowski, 1997), Eppley-VGPM (Carr et al., 2006) and CbPM (Westberry et al., 2008) methodologies. The observation-based estimates are provided with a spatial resolution of ⅙° x ⅙° grid, that is, a 2 160 x 1 080 grid.

42.1.13.1.1 Rates and distribution of nitrogen fixation and denitrification

It is important that the model has a realistic level of nitrogen fixation as the dynamic between diazotrophs and other phytoplankton will influence how the model reacts to nutrient perturbations. Estimates of ocean N_2 fixation have tended to increase over the previous three decades with some key global marine values being (all values provided in Tg N yr^{-1}) 125 ± 41 (Gruber and Sarmiento, 1997); 132 (Codispoti et al., 2001); 121 (Galloway et al., 2004); 135 ± 51 (Gruber, 2004); 140 ± 9 (Luo et al., 2012); and $163 \pm$ 30%49 (Wang et al., 2019).

Alongside work to constrain the scale of global marine N_2 fixation, work has progressed to determine the spatial distribution of diazotrophs. Spatial restrictions on the prevalence of marine nitrogen fixation have been summarised in Figure 2 of Sohm et al. (2011), Figure 3a of Wang et al. (2019), and Figure 4 of Zehr and Capone (2020). In each of these figures marine nitrogen fixation is mostly limited to within 30° either side of the equator. Sohm et al. (2011) and Wang et al. (2019) both indicate that in the Pacific and Atlantic basins nitrogen fixation rates are elevated in the northern hemisphere compared to the southern hemisphere. Wang et al. (2019) and Zehr and Capone (2020) highlight that whilst marine nitrogen fixation is mostly limited to a band from 30° N to 30° S it is somewhat reduced at the equator, and this is particularly so in the Pacific Ocean. The area of reduced nitrogen fixation in the equatorial Pacific Ocean corresponds to an area of nutrient supply from deep water upwelling.

Estimates of denitrification are routinely greater than those for N_2 fixation in marine nitrogen budgets. Example of annual global marine denitrification are 175 ± 28 (Gruber and Sarmiento, 1997); 450 (Codispoti et al., 2001); 322 (Galloway et al., 2004); 245 ± 54 (Gruber, 2004); and $200 \pm$ 26%52 (Wang et al., 2019) (all values provided in Tg N yr^{-1}). Wang et al. (2019) provide location of fixed nitrogen loss due to (a) water column denitrification and anammox and (b) sedimentary denitrification and anammox. Areas of significant water column denitrification include the northern Indian Ocean, northern Pacific Ocean, eastern equatorial Pacific Ocean and the eastern equatorial Atlantic Ocean (Wang et al., 2019). Sedimentary denitrification is more evenly distributed across the ocean basins with intensification closer to coastal locations (Wang et al., 2019).

Comparison techniques

WOA and Ocean Productivity datasets are re-gridded both horizontally and vertically to match NutGEnIE prior to comparison. Hereafter comparisons which utilise the re-gridded datasets are referred to as WOAR and OPR for WOA and Ocean Productivity respectively.

565 Thermohaline transects are used to represent and compare properties of the ocean interior following a similar approach to that detailed by Yool et al. (2021). The aim of the transects is to generally follow water masses from recently ventilated young deep water in the North Atlantic, through the Southern Ocean, to older deep waters in the North Pacific, and basin zonal means are used throughout the transect. For reference, NutGEnIE age of water (i.e., years since ventilation) details are provided in Fig. S4.

570 42.1.33.1.3 **Statistical evaluation**

The alignment processes detailed in the previous two sections also facilitated statistical analysis of properties common to NutGEnIE and WOAR, that is temperature, salinity, [PO_4^-~~PO_4~~], [NO_3^-] and [O_2]. The statistical analysis was conducted for the surface ocean as well as for the thermohaline transects. The statistical calculation only considers cells that are present in both the NutGEnIE and WOAR datasets and computes the mean and standard deviation for each dataset. Correlation analysis

575 between the two datasets can then provide a Pearson correlation coefficient (r) and a p-value resulting from a test of the null hypothesis that there is no relationship between the datasets.

Normalising each dataset by calculating the ratio of each model standard deviation to the observed standard deviation, when combined with correlation coefficients, allows a graphical representation of the skill of NutGEnIE using a Taylor diagram (Taylor, 2001). The normalised NutGEnIE standard deviation will vary either side of 1, with a value of 1 indicating the same

580 standard deviation in the model results as in the observed data. The correlation is indicated by the r value, angular distance θ from the origin is controlled by the normalised standard deviation and the correlation coefficient, with a correlation of 1 on the x-axis. The normalised centred root-mean-square (RMS) difference between NutGEnIE results and observed data is proportional to the distance from points on the plot of perfect agreement.

42.1.43.1.4 **Spatial variation of limiting factors and nutrients**

585 Given the proposed use of the model to investigate the nature of nutrient limitation, additional diagnostic outputs have been added. The diagnostics are based on the nutrient uptake equations for other phytoplankton and diazotrophs (Eq. (9 and 10) respectively). The temperature component γ^T can have values greater than one, therefore the temperature limiting factor (LF_{Temp}) is determined as the minimum of γ^T and 1. This ensures that LF_{Temp} only detects scenarios where temperature acts to constrain nutrient uptake. It is then possible to represent each of these limiting factors on a single figure by setting them

590 each to represent a channel of RGB colour. Nutrient limitation is represented by green; temperature limitation is represented by red; and light limitation is represented by blue. Limitation by multiple factors is represented by the resulting mixed colour as displayed on the Maxwell triangle. The limiting factor values are calculated as follows at each time step of the model processing.

$$LF_{Temp} = \min[\gamma^T, 1] \tag{~~19~~23}$$

595
$$LF_{Light} = \gamma^I \tag{~~20~~24}$$

$$LF_{Nut}^{OPhy} = \min\left[\frac{PO_4^-~~PO_4~~}{PO_4^-~~PO_4~~+K_P}; \frac{DIN}{DIN+K_N}; \frac{Fe}{Fe+K_{Fe}}\right] \tag{~~21~~25}$$

$$LF_{Nut}^{Diaz} = \min\left[\frac{PO_4^-~~PO_4~~}{PO_4^-~~PO_4~~+K_P}; \frac{Fe}{Fe+K_{Fe}^{Diaz}}\right] \tag{~~22~~26}$$

In a similar manner, the limiting nutrient at each time step of model processing is determined by considering each Michaelis-Menten term; this facilitates determination of the PLN at each time step. For each cell and time step the nutrient identified as

19

600 the PLN is assigned 1, the other nutrients are assigned 0. This facilitates the determination of a limiting nutrient term (e.g., LN_P^{OPhy}) as outlined in Eq. (23 to 27).

$$if \ \frac{PO_4^-}{PO_4^-+K_P} < \frac{DIN}{DIN+K_N} \ and \ \frac{PO_4^-}{PO_4^-+K_P} < \frac{Fe}{Fe+K_{Fe}} \ then \ LN_P^{OPhy} = 1 \ else \ LN_P^{OPhy} = 0 \qquad (\text{23}\underline{27})$$

$$if \ \frac{DIN}{DIN+K_N} < \frac{PO_4^-}{PO_4^-+K_P} \ and \ \frac{DIN}{DIN+K_N} < \frac{Fe}{Fe+K_{Fe}} \ then \ LN_N^{OPhy} = 1 \ else \ LN_N^{OPhy} = 0 \qquad (\text{24}\underline{28})$$

$$if \ \frac{Fe}{Fe+K_{Fe}} < \frac{PO_4^-}{PO_4^-+K_P} \ and \ \frac{Fe}{Fe+K_{Fe}} < \frac{DIN}{DIN+K_N} \ then \ LN_{Fe}^{OPhy} = 1 \ else \ LN_{Fe}^{OPhy} = 0 \qquad (\text{25}\underline{29})$$

605 $$if \ \frac{PO_4^-}{PO_4^-+K_P} < \frac{Fe}{Fe+K_{Fe}^{Diaz}} \ then \ LN_P^{Diaz} = 1 \ else \ LN_P^{Diaz} = 0 \qquad (\text{26}\underline{30})$$

$$if \ \frac{Fe}{Fe+K_{Fe}^{Diaz}} < \frac{PO_4^-}{PO_4^-+K_P} \ then \ LN_{Fe}^{Diaz} = 1 \ else \ LN_{Fe}^{Diaz} = 0 \qquad (\text{27}\underline{31})$$

For each nutrient, annual mean values are then calculated for each cell. The PLN is then represented on a figure that utilises a RGB colour mechanism in which Fe PLN is represented by green, $PO_4$$PO_4$ PLN is represented by red, and $NO_3^-$$NO_3$ PLN is represented by blue.

610 ~~42.1.5~~3.1.5 **Model initialisation and steady state.**

The NutGEnIE spin up experiment was executed for 50 kyr, sufficient for the N, P and Fe cycles to reach equilibrium and in excess of the residence time of each nutrient. The concentrations of global mean nutrients and dissolved oxygen throughout that spin up are provided in Fig. S5. The end state concentrations of nutrients and dissolved oxygen are as follows: global mean $[PO_4^-$$PO_4]$ = 2.14 micromoles per kilogram (μmol kg^{-1}); global mean $[NO_3^-$$NO_3]$ = 28.5 μmol kg^{-1}; global mean [TDFe]

615 = 0.73 micromoles per kilogram (nmol kg^{-1}); and global mean $[O_2]$ = 176 μmol kg^{-1}. The NutGEnIE budget for each nutrient at steady state at the end of the 50 kyr spin up experiment is shown below.
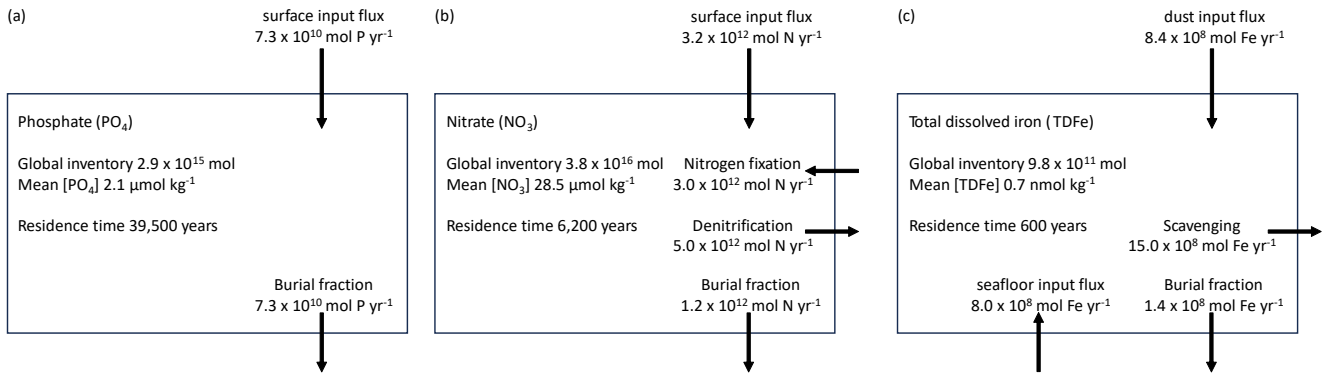
Figure 4 NutGEnIE nutrient budgets at end of 50 kyr spin up. (a) Phosphate budget. (b) Nitrate budget. (c) Total dissolved iron budget. Fluxes into and out of the ocean as a whole are shown, internal ocean cycling through nutrient uptake, remineralisation and nitrification are
620 not shown.
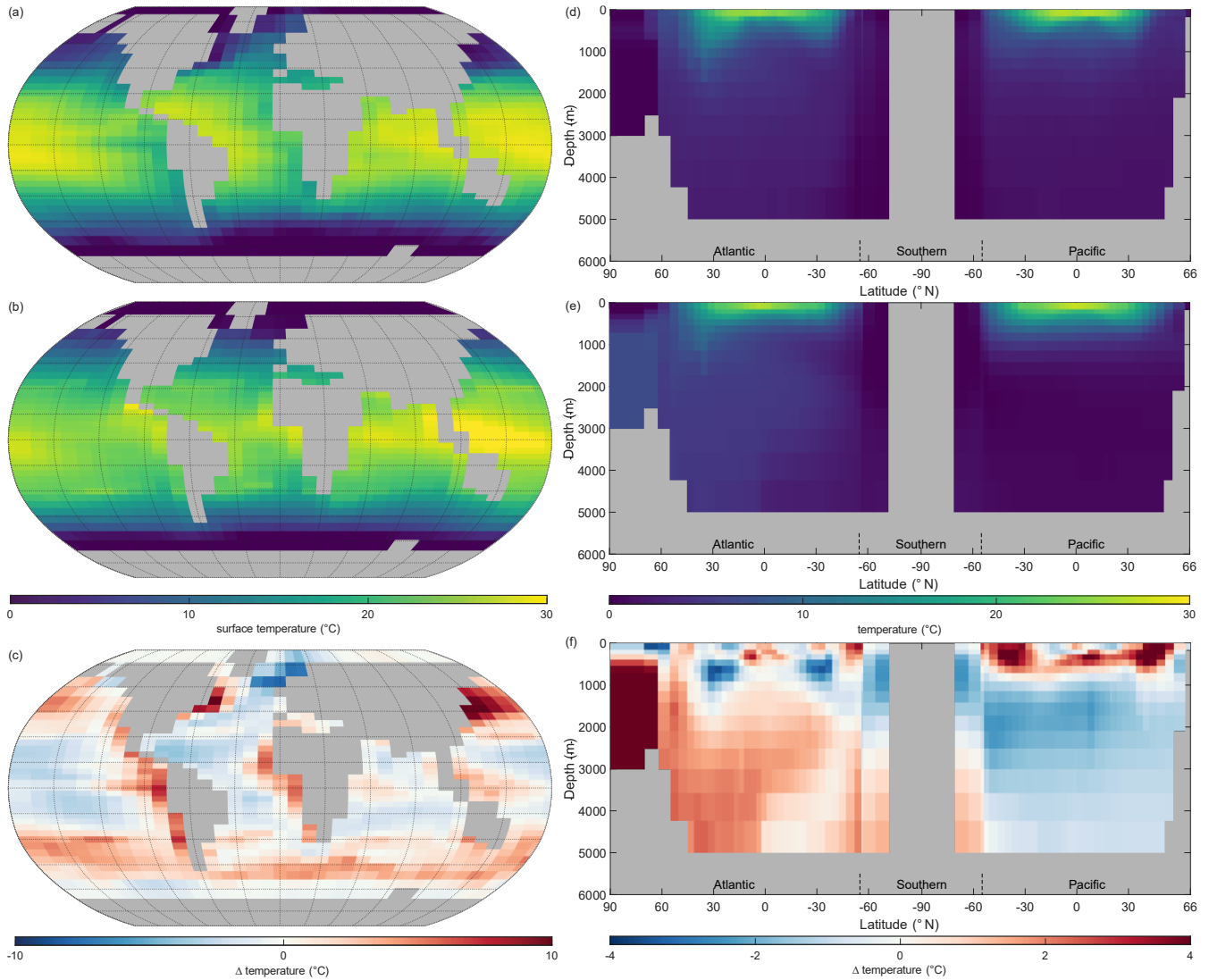
42.23.2 Physical evaluation

Figure 5 Annual mean global temperature. (a) ~~Observed (WOAR)~~Observed World Ocean Atlas Re-gridded (WOAR) sea surface temperature (SST). (b) NutGEnIE SST. (c) Delta SST (NutGEnIE - WOAR). (a-c) based on surface level 0 – 80.8 m depth level. (d) Observed (WOAR) thermohaline transect zonal mean temperature. (e) NutGEnIE thermohaline transect zonal mean temperature. (f) Thermohaline transect temperature delta (NutGEnIE - WOAR). Temperature (and difference) in °C.

Figure 5~~Figure 5~~ shows the observations from the WOAR dataset, NutGEnIE results and deltas (differences between the two) for annual mean global sea surface temperature and thermohaline transects. It is noted that WOAR temperatures are in situ temperature, whereas potential temperature is used in NutGEnIE; however, the differences will be minimal and do not require an alignment conversion. NutGEnIE results are compared to WOAR salinity data in Fig. 6. NutGEnIE represents temperature and salinity reasonably well, but ocean physics is not the focus here, so the properties are not described in detail. Mean surface and interior (thermohaline transect) temperature and salinity values for both NutGEnIE and WOAR are provided in Table 7~~Table 6~~. NutGEnIE does exhibit some temperature biases; positive surfaces biases are present in the north and south Pacific with a negative surface bias in the Pacific subtropics (Fig 5 c). Similarly, biases exist in the temperature transect (Fig 5 f); for example, NutGEnIE has a general positive bias in the deep Atlantic and Southern Ocean. In the deep Pacific, NutGEnIE has a negative bias. Salinity biases of NutGEnIE are generally of low magnitude, within 1 psu. Surface biases (Fig. 6 c) can be summarised as positive at higher latitudes and negative at mid latitudes. NutGEnIE salinity at depth greater than 1 000 m have a positive bias with generally negative biases in the upper 500 m (Fig. 6 f).

21
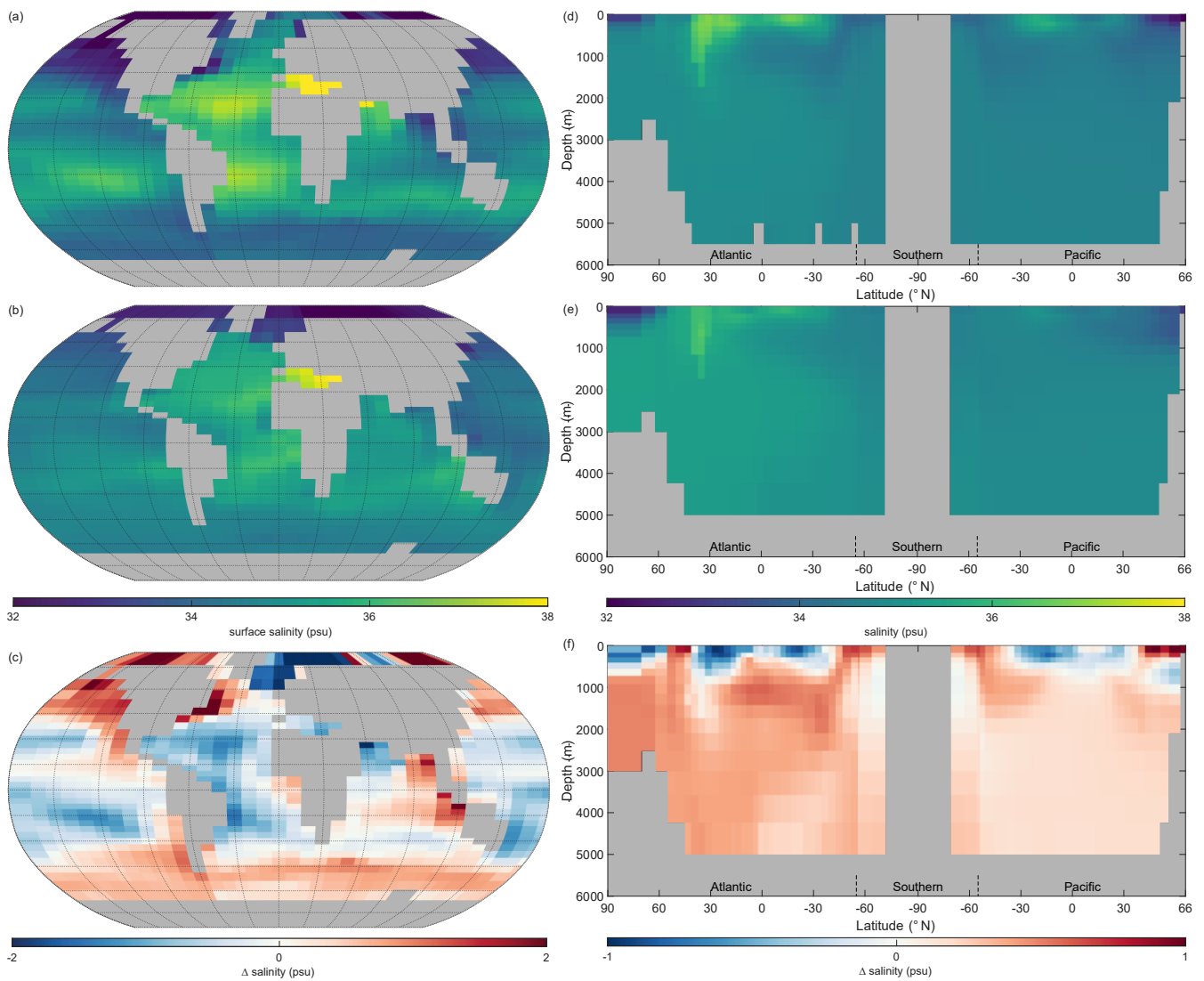
Figure 6 Annual mean global salinity. (a) ~~Observed (WOAR)~~Observed World Ocean Atlas Re-gridded (WOAR) sea surface salinity (SSS). (b) NutGEnIE SSS. (c) Delta SSS (NutGEnIE - WOAR). (a-c) based on surface level 0 – 80.8 m depth level. (d) Observed (WOAR) thermohaline transect zonal mean salinity. (e) NutGEnIE thermohaline transect zonal mean salinity. (f) Thermohaline transect salinity delta (NutGEnIE - WOAR). Salinity (and difference) in psu.

~~42.3~~3.3 Biogeochemistry tracer evaluation (nutrients, oxygen)

~~42.3.1~~3.3.1 Phosphate

The representation of phosphate and the other nutrients by NutGEnIE is particularly important if the model is to be suitable for experiments that examine the impacts of variations in nutrient supply. We have seen that the end state global mean concentration of phosphate is 2.14 μmol kg^{-1}; we now consider the spatial variation and compare to observational data.

The surface phosphate concentrations of NutGEnIE are largely a good representation of the observed concentration from WOAR. In general, NutGEnIE surface [PO_4^-~~PO_4~~] is slightly greater than observed [PO_4^-~~PO_4~~] at low latitudes and slightly less than observed [PO_4^-~~PO_4~~] at higher latitudes (Fig. 7 a-c). The magnitude of differences in surface [PO_4^-~~PO_4~~] between NutGEnIE and observations are almost universally less than 0.5 μmol kg^{-1}. There are some specific differences to be noted; NutGEnIE surface [PO_4^-~~PO_4~~] is lower than observed in the North Pacific; between 45° S and 60° S NutGEnIE surface [PO_4^-~~PO_4~~] is lower than observed; and NutGEnIE does not fully represent the supply of nutrients in upwelling areas of the equatorial Pacific and Benguela. The mean NutGEnIE annual mean global surface [PO_4^-~~PO_4~~] is 0.52 μmol kg^{-1} with a standard deviation of 0.36 which compare to WOAR mean and standard deviations of 0.58 and 0.54 μmol kg^{-1} respectively.
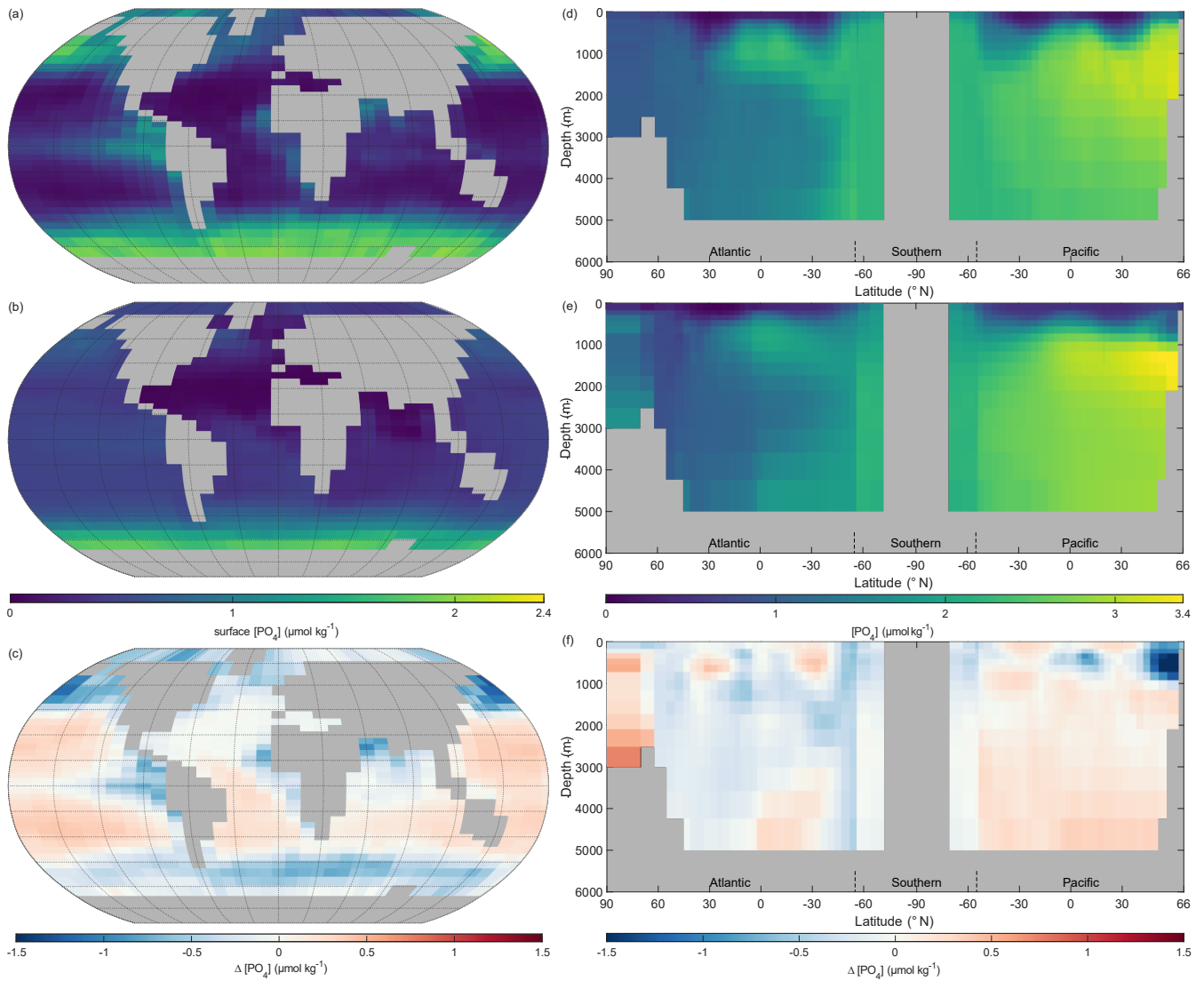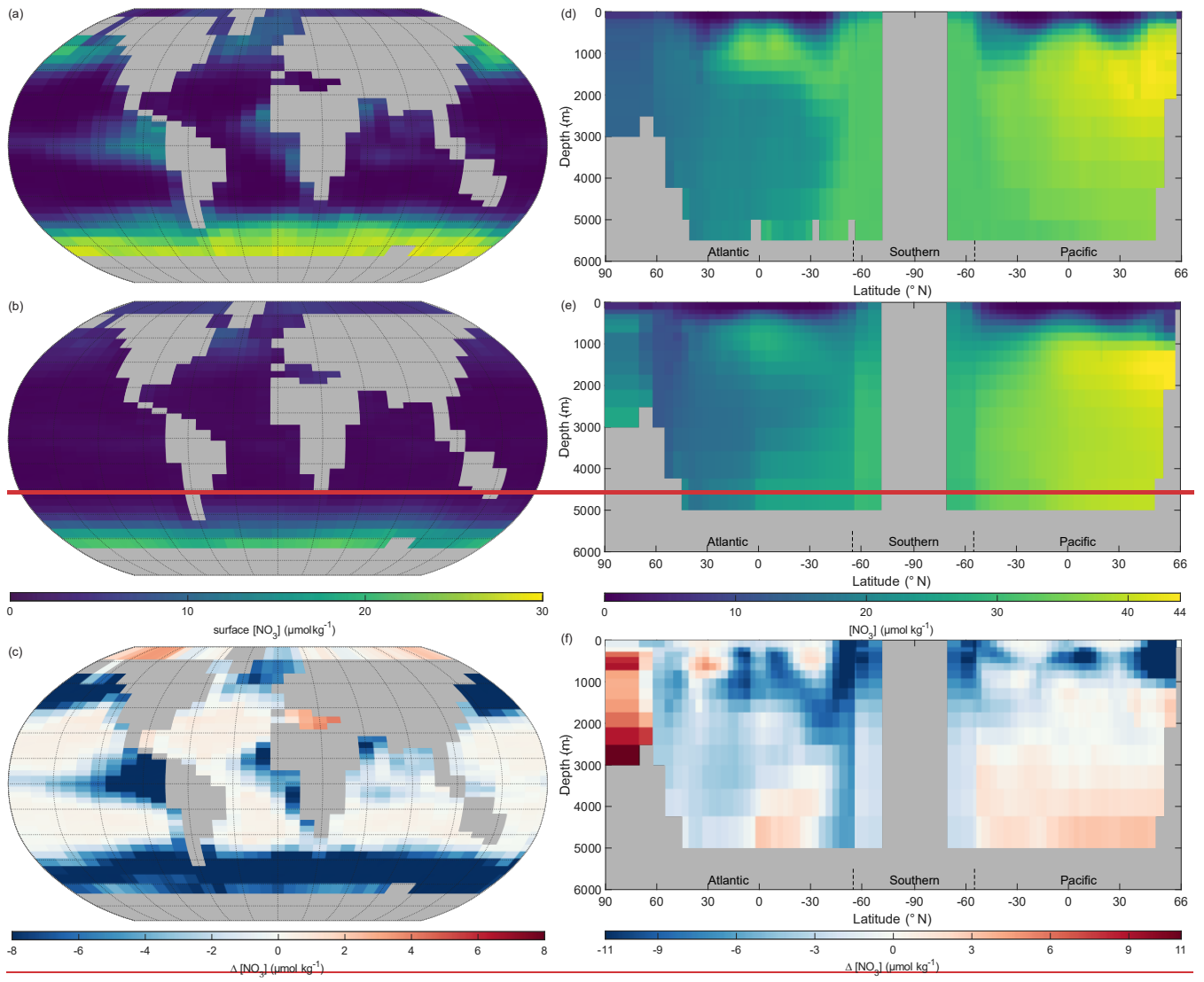
22
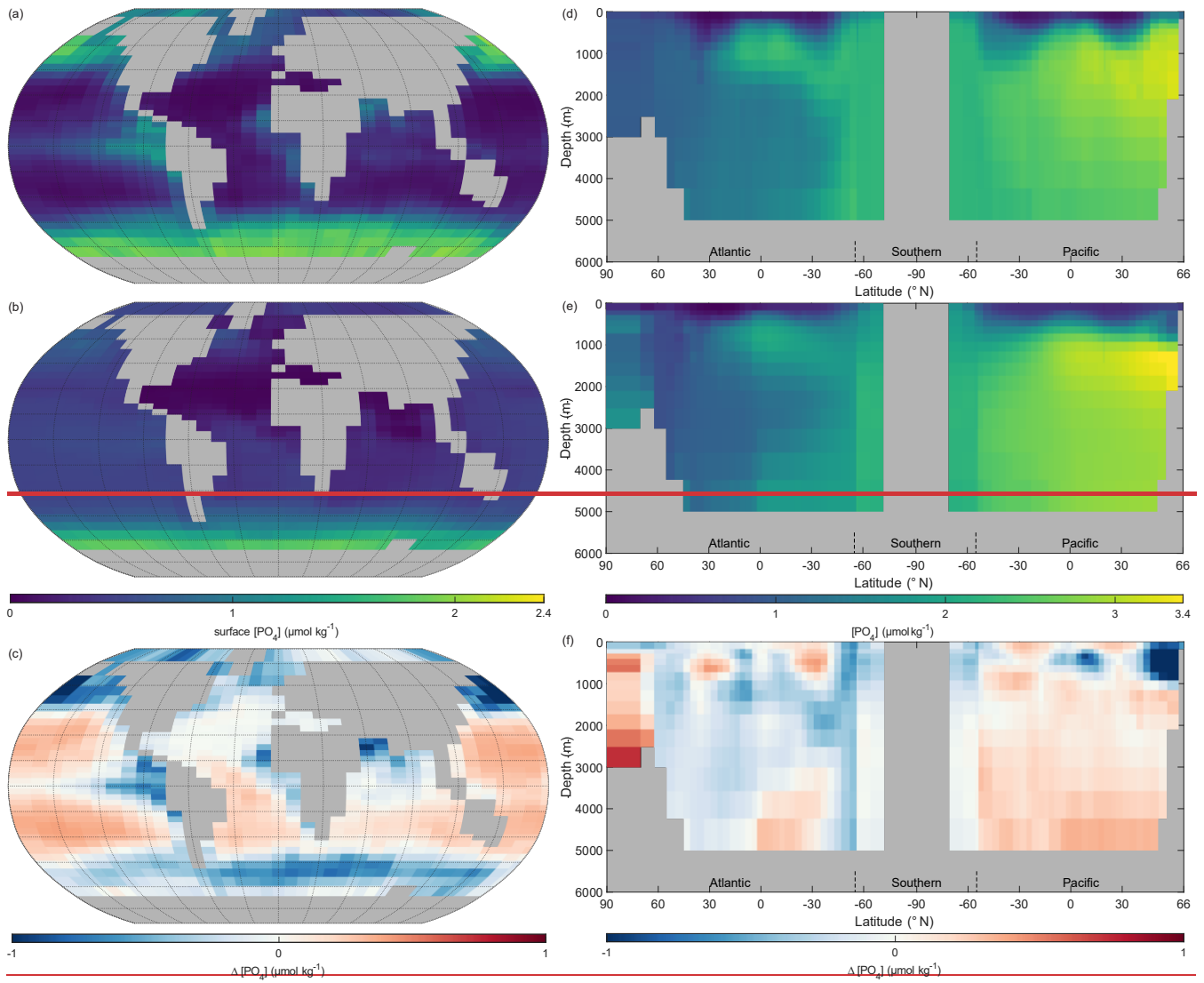
Figure 7 Annual mean global phosphate concentration ([PO̶4̶PO₄]). (a) ~~Observed (WOAR)~~Observed World Ocean Atlas Re-gridded (WOAR) surface [PO̶4̶PO₄]. (b) NutGEnIE surface [PO̶4̶PO₄]. (c) Delta surface [PO̶4̶PO₄] (NutGEnIE - WOAR). (a-c) based on surface level 0 – 80.8 m depth level. (d) Observed (WOAR) thermohaline transect zonal mean [PO̶4̶PO₄]. (e) NutGEnIE thermohaline transect zonal mean [PO̶4̶PO₄]. (f) Thermohaline transect [PO̶4̶PO₄] delta (NutGEnIE - WOAR). [PO̶4̶PO₄] (and difference) in µmol kg⁻¹.

Ocean interior representation of phosphate by NutGEnIE is also successfully aligned to observed concentrations (Fig. 7 (d to f)). The <u>ocean interior</u> Atlantic sector has somewhat lower [PO̶4̶PO₄] than the Southern Ocean and [PO̶4̶PO₄] is further elevated in the Pacific Ocean, reflecting the age of water masses, and increasing remineralisation <u>(Fig. 7e)</u>. NutGEnIE also represents well the differing water masses in the Atlantic Ocean with the tongue of northward flowing Antarctic Intermediate Water rich in nutrients. Differences between NutGEnIE and observations are minimal apart from the northern Pacific Ocean at depths less than 1 000 m where NutGEnIE [PO̶4̶PO₄] are approximately 1.2 µmol kg⁻¹ less than observed concentrations. In general, NutGEnIE has a slight negative bias in [PO̶4̶PO₄] in the Atlantic Ocean and a slight positive bias in [PO̶4̶PO₄] in the Pacific Ocean. NutGEnIE represents the [PO̶4̶PO₄] in the Southern Ocean in alignment with observations and there are consequently minimal differences in that sector of the thermohaline transect. The mean NutGEnIE annual mean [PO̶4̶PO₄] of the thermohaline transect is 2.0 µmol kg⁻¹ with a standard deviation of 0.73 µmol kg⁻¹ which compare to WOAR mean and standard deviations of 2.0 and 0.64 µmol kg⁻¹ respectively.

~~4.3.2~~3.3.2 Nitrate

Surface nitrate concentrations of NutGEnIE largely follow the spatial patterns of the observed concentration (Fig. 8 (a to c)). In general, NutGEnIE surface [NO̶3̶NO₃] are lower than the observed [NO̶3̶NO₃], although this is less evident at low latitudes. The magnitude of differences in surface [NO̶3̶NO₃] between NutGEnIE and observations are almost universally less than 10

24

µmol kg^{-1}. There are some specific differences to be noted which are similar to those identified for phosphate; NutGEnIE

680   surface [$NO_3$$\overline{NO_3}$] are lower than observed in the North Pacific; between 45° S and 60° S NutGEnIE surface [$NO_3$$\overline{NO_3}$] are

≈ 10 µmol kg^{-1} lower than observed; and NutGEnIE does not fully represent the supply of nutrients in upwelling areas of the

equatorial Pacific and Benguela. The mean NutGEnIE annual mean global surface [$NO_3$$\overline{NO_3}$] is 3.0 µmol kg^{-1} with a standard

deviation of 4.68 µmol kg^{-1} which compare to WOAR mean and standard deviations of 6.0 and 7.99 µmol kg^{-1} respectively.

(a)

(b)

(c)

(d)

(e)

(f)

surface [NO$_3$] (µmol kg^{-1})

[NO$_3$] (µmol kg^{-1})

Δ [NO$_3$] (µmol kg^{-1})

Δ [NO$_3$] (µmol kg^{-1})

Depth (m)

Latitude (° N)

Atlantic   Southern   Pacific

26

Figure 8 Annual mean global nitrate concentration ([~~NO₃⁻NO₃~~]). (a) ~~Observed (WOAR)~~Observed World Ocean Atlas Re-gridded (WOAR) surface [~~NO₃⁻NO₃~~]. (b) NutGEnIE surface [~~NO₃⁻NO₃~~]. (c) Delta surface [~~NO₃⁻NO₃~~] (NutGEnIE - WOAR). (a-c) based on surface level 0 – 80.8 m depth level. (d) Observed (WOAR) thermohaline transect zonal mean [~~NO₃⁻NO₃~~]. (e) NutGEnIE thermohaline transect zonal mean [~~NO₃⁻NO₃~~]. (f) Thermohaline transect [~~NO₃⁻NO₃~~] delta (NutGEnIE - WOAR). [~~NO₃⁻NO₃~~] (and difference) in µmol kg⁻¹.

Ocean interior representation of nitrate by NutGEnIE are aligned to observation concentrations (Fig. 8 (d to f)). The Atlantic sector has somewhat lower [~~NO₃⁻NO₃~~] than the Southern Ocean and [~~NO₃⁻NO₃~~] are further elevated in the Pacific Ocean, this again reflects the age of water masses, and increasing remineralisation. NutGEnIE also successfully represents differing water masses in the Atlantic Ocean with the tongue of northward flowing Antarctic Intermediate Water rich in nutrients. Differences between NutGEnIE and observations are less than 5 µmol kg⁻¹ apart from the northern Pacific Ocean at depths less than 1 000 m where NutGEnIE [~~NO₃⁻NO₃~~] are as much as 18 µmol kg⁻¹ less that observed concentrations. In general, NutGEnIE has a positive bias in [~~NO₃⁻NO₃~~] in the Arctic, a negative bias in the Atlantic Ocean, a minimal negative bias in the Southern Ocean, and a positive bias in [~~NO₃⁻NO₃~~] in the Pacific Ocean below 1 000 m. The mean NutGEnIE annual mean [~~NO₃⁻NO₃~~] of the thermohaline transect is 26.5 µmol kg⁻¹ with a standard deviation of 9.95 µmol kg⁻¹ which compare to WOAR mean and standard deviations of 28.3 and 9.0 µmol kg⁻¹ respectively.

~~4.2.3.3~~3.3.3 Iron

In general, NutGEnIE broadly represents the observed iron depth profiles from the four GEOTRACES cruises (Fig. 9). A sample of 6 profiles for each cruise are shown here (the complete set of depth profiles for each cruise are available in supplementary information Fig. S6 to S24). The simplified bathymetry associated with the NutGEnIE 36 x 36 x16 structure does result in several profiles where the depth of the NutGEnIE grid cell is significantly shallower than the specific ocean

27

705 depth, for example Fig. 9(a) profile (6) and Fig. 9(c) profile (2). There are, however, a total of 107 profiles across the four cruises which provide sufficient opportunities to consider the ability of NutGEnIE to represent ocean iron concentrations. It is important to note that the GEOTRACES based profiles represent a specific point in time whereas the NutGEnIE profiles represent annual mean concentrations.

There are 47 profiles associated with cruise GA02 covering a transect in the Atlantic Ocean from 64° N to 60° S. There are
710 two instances where the depth profiles of NutGEnIE do not follow the observed profiles. Firstly, where the observed profile has a subsurface peak or maximum in the TDFe concentration (e.g., Fig. 9(a) profile (13)). Secondly, where the observed profile has an elevated surface TDFe concentration (e.g., Fig. 9(a) profile (34)), potentially related to an episodic input of iron from dust. At depths below 1 000 m the there is strong alignment between the NutGEnIE profiles and the observed profiles.

Figure 9 Sample iron depth profiles for GEOTRACES cruises. (a) NutGEnIE and GEOTRACES GA02 cruise. (b) NutGEnIE and GEOTRACES GIPY05 cruise. (c) NutGEnIE and GEOTRACES GPc06 cruise. (d) NutGEnIE and GEOTRACES GP19 cruise. (a-d) Total dissolved iron (TDFe) in nmol kg^{-1}. Blue line represents GEOTRACES observations of [TDFe], red dashed line represents NutGEnIE [TDFe]. e) Location of GEOTRACES cruises and stations used here for comparison to the NutGEnIE model. Cruise station locations are shown as follows: GPc06 – red diamonds, GP19 – black circles, GA02 - blue squares and GIPY05 – magenta triangles.

29

There are 35 profiles associated with cruise GIPY05 covering two transects in the Atlantic sector of the Southern Ocean. The latitude range of these profiles is between 42° S and 68° S with longitudes ranging between 66° W and 9° E. There are some profiles where NutGEnIE does not accurately represent the observed profiles; examples include Fig. 9(b) profiles (8), (9), and (26). However, as with cruise GA02, NutGEnIE depth profiles of TDFe associated with cruise GIPY05 provide a reasonable representation of the observed depth profiles.

GEOTRACES cruise GPc06 and GP19 were both undertaken in the Pacific Ocean and have 12 and 13 depth profiles of TDFe, respectively. Cruise GPc06 covered a range of latitudes from 54° N to 10° S at a longitude of 200° E. The TDFe depth profiles associated with cruise GPc06 (Fig. 9(c)) highlight reasonable alignment between NutGEnIE and the observed TDFe concentrations. The one exception to this is profile (11) where the observed profile shows elevated [TDFe] between 100 and 1 000m. This profile is the most northerly, 54° N, and associated with an area of the North Pacific where NutGEnIE is less accurate in the representation of both phosphate and nitrate (Fig. 7 and 8 respectively).

Cruise GP19 covered the more southerly latitudes of the Pacific Ocean from the equator to 64° S at a longitude of 200° E. One profile occurs when the cruise travelled to a more westerly location at 30° S, 174° E. The TDFe depth profiles associated with cruise GP19 (Fig. 9(d)) highlight reasonable alignment between NutGEnIE and the observed TDFe concentrations. In summary the depth profiles of TDFe concentrations associated with GEOTRACES cruises GA02, GIPY05, GPc06, and GP19 indicate that NutGEnIE can successfully reflect average observations.

For each of the 107 depth profiles mean values of [TDFe] were calculated for both GEOTRACES and NutGEnIE. For these profiles the NutGEnIE mean [TDFe] ranged from 0.45 to 0.90 nmol kg^{-1}. The mean [TDFe] for GEOTRACES ranged from 0.16 to 1.25 nmol kg^{-1}. The NutGEnIE mean [TDFe] were on average 0.14 nmol kg^{-1} higher than measurements GEOTRACES recorded. The focus here has been to compare NutGEnIE results to ocean observations, and this has been done using GEOTRACES depth profiles because WOA does not contain [TDFe] data. In addition, NutGEnIE [TDFe] for the surface ocean and thermohaline transect are provided in Fig. S25.

42.3.43.3.4 Dissolved oxygen

It is known that gas solubility in seawater is a function of temperature, with gas solubility inversely correlated to temperature. Therefore, oxygen dissolves more readily in cooler seawater. It follows that the highest concentrations of surface dissolved oxygen should be observed in high latitude water and the surface dissolved oxygen reduce in each hemisphere moving towards the equator (Fig. 10 (a)). The representation of surface dissolved oxygen by NutGEnIE also reflects the variation by latitude, with the maximum concentrations in the Arctic Ocean followed by the Southern Ocean. The difference figure (Fig. 10 (c)), highlights that in general NutGEnIE has higher dissolved oxygen concentrations than observed. There are areas of the latitude ranges 30° N to 60° S and 30° N to 60° S in which NutGEnIE dissolved oxygen concentrations are lower than observed. Region where NutGEnIE dissolved oxygen concentrations are higher than observed (> 40 µmol kg^{-1}) are the North Atlantic to the east of Greenland, the northern Indian Ocean and the equatorial upwelling regions of the eastern Pacific and Indian Oceans. The mean NutGEnIE annual mean global surface [O$_2$] is 249 µmol kg^{-1} with a standard deviation of 44.60 µmol kg^{-1} which compare to WOA mean and standard deviations of 239 and 44.64 µmol kg^{-1} respectively.

When considering the ocean interior (Fig. 10 (d to f)) and comparing the observed dissolved oxygen concentrations to those of NutGEnIE it is again the case that NutGEnIE largely reflects the observed spatial variations. The Atlantic sector in both the observed and NutGEnIE transects have generally higher dissolved oxygen concentrations than the Pacific Ocean, reflecting the fact the Pacific Ocean contains older water into which there has been greater remineralisation of organic matter. The tongue of AAIW with reduced dissolved oxygen concentrations is evident in both the observed and NutGEnIE transects. In both the observed and NutGEnIE transects the highest dissolved oxygen concentrations are seen towards the surface at high latitudes, that is, the Arctic Ocean, Southern Ocean, and North Pacific. The minimum dissolved oxygen concentrations, approaching 100 µmol kg^{-1} are in the North Pacific at depths up to 3 000m in both the observed and NutGEnIE transects. However,

NutGEnIE does not reflect the observed dissolved oxygen concentrations in the Arctic Ocean at depth well, with concentrations greater than 40 µmol kg^{-1} below the observed concentrations. In addition, NutGEnIE tends to have higher concentrations of dissolved oxygen (by up to 40 µmol kg^{-1}) in the upper 2 000 m of the water column and lower concentrations of dissolved oxygen (by up to 40 µmol kg^{-1}) at greater depths. The mean NutGEnIE annual mean global interior [O$_2$] is 189 µmol kg^{-1} with a standard deviation of 55 which compare to WOAR mean and standard deviations of 194 and 65 µmol kg^{-1} respectively.

Figure 10 Annual mean global dissolved oxygen ([O$_2$]). (a) ~~Observed (WOAR)~~Observed World Ocean Atlas Re-gridded (WOAR) surface [O$_2$]. (b) NutGEnIE surface [O$_2$]. (c) Delta surface [O$_2$] (NutGEnIE - WOAR). (a-c) based on surface level 0 – 80.8 m depth level. (d) Observed (WOAR) thermohaline transect zonal mean [O$_2$]. (e) NutGEnIE thermohaline transect zonal mean [O$_2$]. (f) Thermohaline transect [O$_2$] delta (NutGEnIE - WOAR). [O$_2$] (and difference) in µmol kg^{-1}.

~~42.3.5~~3.3.5 Statistical analysis results

Statistical information, such as mean values, have in many cases been provided alongside the results associated with each ocean property; here we summarise the statistical and correlation results.

For all variables there is good agreement between the NutGEnIE and WOAR mean values; all NutGEnIE means are within one standard deviation of the observed WOAR mean. The NutGEnIE datasets are derived from less granular grids and therefore it is understandable that in most cases the associated standard deviations are lower than the WOAR standard deviation. Correlation coefficients between NutGEnIE and WOAR are reassuring with values ranging from 0.76 (surface [O$_2$]) to 0.97 (surface temperature). In all cases the correlation p-values are zero, indicating strong rejection of the null hypothesis that the NutGEnIE and WOAR datasets are not correlated. Histograms of the NutGEnIE and WOAR datasets for each of the variables

in Table 7~~Table 6~~ also show reassuring similarities (supplementary information Fig. S26 to S35). A graphical representation of the skill of NutGEnIE can by visualised using a Taylor diagram, Fig. 11.

Table 76 Statistical comparison of NutGEnIE to WOAR. Surface values relate to level depth of 0 - 80.8 m. Interior values reflect the thermohaline transects as defined in Sect. 3.1.2. sd = standard deviation. All correlations have a p-value of 0.

Variable (units)	$PO_4^-$$PO_4$ (µmol kg^{-1})		$NO_3^-$$NO_3$ (µmol kg^{-1})		temperature (°C)		salinity (psu)		O_2 (µmol kg^{-1})	
	Surface	Interior	Surface	Interior	Surface	Interior	Surface	Interior	Surface	Interior
WOAR mean	0.58	12.96	6.0	28.3	17.5	3.2	35	35	240	194
NutGEnIE mean	0.52	12.96	32.09	26.6	18.1	3.5	35	35	249	189
WOAR sd	0.54	0.64	7.99	9.00	9.56	3.72	1.19	0.33	52.91	64.55
NutGEnIE sd	0.36	0.73	4.68	9.95	9.06	4.05	0.78	0.34	44.64	54.62
Pearson correlation coefficient (r)	0.82	0.92	0.88	0.90	0.97	0.93	0.77	0.82	0.94	0.76

Figure 11 Taylor diagram of NutGEnIE and ~~observed (WOAR)~~Observed World Ocean Atlas Re-gridded (WOAR). Showing surface and interior temperature, salinity, [$PO_4^-$$PO_4$], [$NO_3^-$$NO_3$] and [$O_2$]. The RMS error and standard deviations have been normalised by the observed standard deviation of each field before plotting. Therefore, the RMS error and standard deviation indicate the ratio to the observed standard deviation. Angular distance θ is controlled by the correlation coefficient (r), with a correlation of 1 on the x-axis. The diagrams

show NutGEnIE results to observation (WOAR) comparisons based on annual average spatial fields.

~~42.3.73.3.6~~3.3.6 Rates of PP

It was noted (Sect. 2.2) that NutGEnIE does not explicitly model primary producer (phytoplankton) biomass. Nutrient uptake within the surface layer of NutGEnIE is an output of the model. NutGEnIE nutrient uptake is converted to the units (g C m^{-2}

d^{-1}) of the Observation-based PP provided by the Oregon State University Ocean Productivity group (Ocean Productivity, 2024) and shown below (Fig. 12). A direct quantitative comparison is not appropriate because NutGEnIE nutrient uptake is

Large areas of the oceans away from the continental land masses have low levels of PP and this is reflected in both observations

805   and NutGEnIE (Fig. 12). A figure showing the base Ocean Productivity dataset prior to re-gridding is available in Fig. S36. PP is enhanced by upwelling, e.g., the equatorial Pacific and Eastern Atlantic, and this is reflected in both observations and NutGEnIE. However, the highest observed rates of PP are seen immediately adjacent to the continental land masses. These elevated observed rates of PP are unable to be reflected accurately by NutGEnIE given the 36 x 36 spatial resolution. NutGEnIE also overestimates the rate of PP in the North Atlantic in an area south of Greenland and in a band close to 60° S.

Figure 12 Annual mean global primary production. (a) Oregon State University Ocean Productivity (Ocean Productivity, 2024) re-gridded (OPR). (b) NutGEnIE surface layer nutrient uptake converted to units of g C m^{-2} d^{-1}. (a) and (b) A log (base 10) scale is used and units are g C m^{-2} d^{-1}. (c) Difference (NutGEnIE – OPR). Primary production (and difference) in g C m^{-2} d^{-1}.

~~4.2.3.8~~3.3.7 **Nitrogen cycle processes**

The NutGEnIE global mean rate of marine nitrogen fixation is 3.0 x 10^{12} mol N yr^{-1} which equates to 84 Tg N yr^{-1}, with the majority occurring in the low latitudes, within 30° either side of the equator. The distribution of nitrogen fixation and associated rates in μmol N kg^{-1} yr^{-1} can be seen in Fig. 13 (a). Higher rates of nitrogen fixation in each ocean basin are seen north of the equator than south of the equator. The highest rates of nitrogen fixation (4.0 μmol N kg^{-1} yr^{-1}) occur between the equator and 15° N in the Atlantic Ocean. A significant area of the Pacific Ocean either side of the equator has minimal or zero rates of nitrogen fixation.

Denitrification can occur throughout the water column, dependant on the consumption of election acceptors in the process of OM remineralisation as outlined in Sect. 2.3.7. In NutGEnIE denitrification occurs via the decomposition of organic matter ~~by bacteria~~, when oxygen levels are low, which leads to the use of nitrate as an alternative electron acceptor. This in turn results in the conversion of nitrate to dinitrogen ~~(Sect. 2.3.4)~~. NutGEnIE water column integrated denitrification is shown in Fig. 13 (b). The NutGEnIE global mean rate of marine denitrification is 3.2 x 10^{12} mol N yr^{-1} which equates to 90 Tg N yr^{-1}
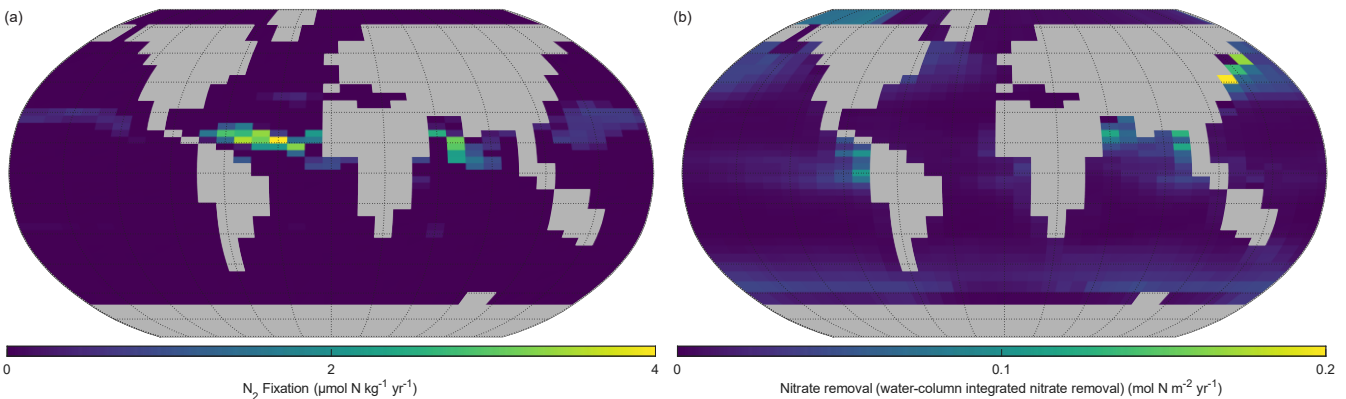

Figure 13 Annual mean distribution of NutGEnIE nitrogen fixation and denitrification. (a) Surface level nitrogen fixation in μmol N kg^{-1} yr^{-1}. (b) water column denitrification.

In addition, Nitrogen* (N^*) (Gruber and Sarmiento, 1997) analysis has been conducted for WOAG and NutGEnIE and provided in Figs. S52 and S53 respectively. The overall trend in N^* for both WOAG and NutGEnIE is that concentrations are highest in the North Atlantic and decrease gradually toward the Pacific. For both WOAG and NutGEnIE this implies a net transport of fixed nitrogen from the Atlantic to the Pacific.

~~4~~3~~4~~ **Discussion**

~~4.3.1~~4.1 **Summary**

We have presented the features of NutGEnIE and carried our comparisons to datasets based on ocean observations. Focus on nutrient cycles and associated biogeochemical cycles has been vital with NutGEnIE compared to both WOAR (phosphate, nitrate and dissolved oxygen) and GEOTRACES (iron) datasets. In addition, the WOA provides temperature and salinity datasets that have been compared with NutGEnIE so give confidence that the fundamental physical properties are being well represented. NutGEnIE has also been qualitatively compared against ocean productivity data from the Oregon State University Ocean Productivity group. For each attribute the comparisons have shown that NutGEnIE is an effective representation rather than a perfect replication of the oceans which would be unrealistic.

The NutGEnIE steady state nutrient global inventories (Fig. 4) are well aligned to ocean estimates; this is also evident in the comparisons of interior nutrient concentrations. Fluxes associated with each NutGEnIE nutrient cycle, considering the simplified cycles, are close to literature estimates of ocean nutrient budgets. NutGEnIE residence times (phosphate ~40,000 years, nitrate ~6,000 years and iron < 1000 years) are of the expected order of magnitude, although iron is slightly higher than

global ocean estimates tens to hundreds years (Delaney, 1998; Gruber, 2004; Hayes et al., 2018). This supports the conclusion that NutGEnIE nutrient cycles as configured here are a reasonably accurate representation of the oceans.

The mechanisms that maintain NutGEnIE ocean nutrient concentrations are pertinent to the intended investigations and, therefore, significant discrepancies would be worrying. Annual mean concentrations of phosphate and nitrate both compare successfully to the WOAR. Those comparisons have considered both the areas with first order impact to ocean PP, that is, the surface ocean and the ocean interior that has longer term impact on PP in terms of nutrient replenishment. In is noted that the mean NutGEnIE annual mean global surface $[NO_3^-]$ is 3.0 µmol kg^{-1} compared to a WOAR value of 6.0 µmol kg^{-1}. NutGEnIE agrees well with WOAR across most of the surface ocean with the discrepancy mainly relating to the Southern Ocean and northern Pacific Ocean. This bias is deemed acceptable as the configuration results in rates of PP, spatial variation of nutrient limitation (Sect. 4.2), nitrogen cycle dynamics and other properties that have good validation results. Differences in both nutrients' concentrations have been identified and noted; however, there are no significant flaws in NutGEnIE distributions related to phosphate and nitrate.

NutGEnIE's global mean rate of marine nitrogen fixation and denitrification are 84 Tg N yr^{-1} and 90 Tg N yr^{-1} respectively these are both lower than ocean estimates, for example, these NutGEnIE global rates are 67% and 52% of the Gruber and Sarmiento (1997) estimates. The spatial distributions of NutGEnIE nitrogen fixation and denitrification are encouraging and alongside N^* analysis (Fig. S52 and S53) indicate that NutGEnIE largely represents the nitrogen fixation and denitrification processes well. Apparent Oxygen Utilisation (AOU) analysis can give an insight into biological processes, primarily through respiration/remineralisation, that consume oxygen see Fig. S50 and S51. The similarity of the WOAR and NutGEnIE AOU transects give additional reassurance that the rate of export and subsequent remineralisation processes in NutGEnIE are realistic.

In summary, the validation of NutGEnIE results against ocean observations suggest that NutGEnIE represents the ocean successfully. In particular, the representation of nutrient concentrations give confidence that NutGEnIE will be suitable for the intended study of long-term influence of nutrients on oceanic PP. There are, however, aspects of NutGEnIE as configured here that do not represent reality as successfully and these are noted below. The representation of the Artic Ocean has highlighted discrepancies relating to temperature, salinity, and dissolved oxygen below the surface. In general, NutGEnIE nutrient concentrations in the upper 1000m of the northern Pacific Ocean are lower than observed concentrations, NutGEnIE biases in this area also exist for temperature, dissolved oxygen and AOU. The derived NutGEnIE NPP used here results in an overestimates PP in an area of the North Atlantic close to Greenland and a band close to 60° S. Whilst these discrepancies are noted, the ability of NutGEnIE to successfully represent Earth's oceans and processes indicate that NutGEnIE will be useful for the future investigations into the long-term influence of nutrients on oceanic primary production.

43.24.2 Spatial variation of limitations

The comparisons to ocean observations detailed in the results have not considered the limiting factors that act to control PP. Here, we briefly review those limiting factors and in particular the spatial variation of nutrient limitation to ensure that NutGEnIE is realistic as these aspects will be vital in the proposed investigations of the ULN.

The nature of light and temperature limitations are such that they exert the greatest restriction on nutrient uptake in the higher latitudes. The comparative limitations of nutrient uptake by light, temperature, and nutrient supply are shown in Fig. 14 for both other phytoplankton and diazotrophs. For both phytoplankton classes a combination of light, temperature, and nutrient supply limit nutrient uptake in the high latitudes. The nutrient uptake at low and mid latitudes is controlled by nutrient availability. The spatial variability of nutrient limitation is shown in Fig. 15 that displays the PLN for each phytoplankton class.

Other phytoplankton nutrient uptake is limited by a combination of nutrients. $PO_4^-$$PO_4$ is the PLN in 1% of the surface ocean, DINNO_3 is the PLN for 71 % and Fe limiting in the remaining 28 %. $PO_4^-$$PO_4$ limitation is restricted to the Mediterranean Sea

890 and a small area of the Caribbean. The areas where Fe acts as the PLN are the Southern Ocean, south of 40° S, and north of 40° N in both the Pacific and Atlantic Oceans.
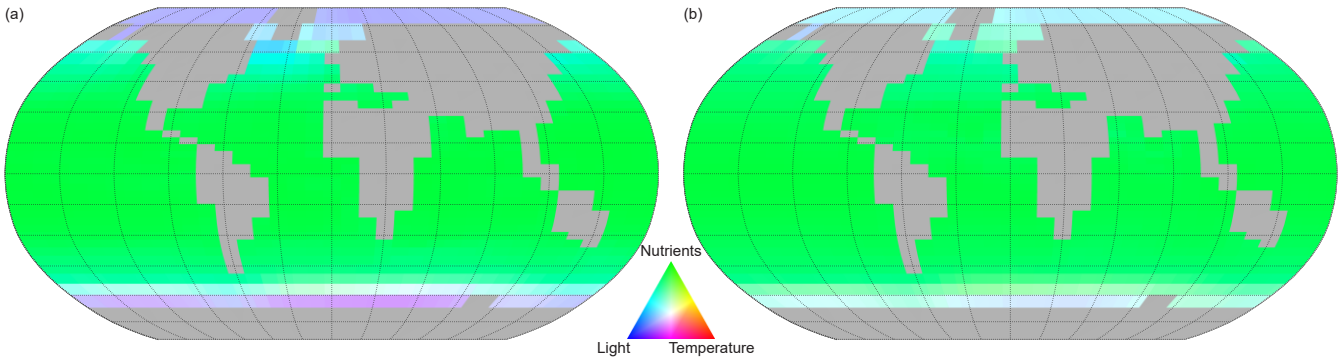

Figure 14 Spatial variation of the limiting factor for nutrient uptake, (a proxy for phytoplankton growth in NutGEnIE). For (a) other phytoplankton and (b) diazotrophs. Red = temperature limitation, green = Nutrient limitation, blue = light limitation.

895 Figure 14Figure 14 facilitates the representation of the three limiting factors on a single figure, however, the colours used are not favourable to readers with colour vision deficiencies. Figures showing individual limiting factors are available in supplementary information Fig. S37 to S45.

Nutrient uptake by diazotrophs will only be limited by either Fe or $PO_4^-$$PO_4$ (dinitrogen is freely available for nitrogen fixation). In this configuration of NutGEnIE, Fe is the PLN for diazotrophs across 93 % of the surface ocean, with $PO_4$$PO_4$ being the

900 PLN in the remaining 7 %. The areas where $PO_4^-$$PO_4$ acts as the PLN for diazotrophs are restricted to the northern hemisphere and are the Atlantic Ocean from 15° N to 40° N; the Mediterranean Sea; and a section of the Indian Ocean from the equator to 30° N.
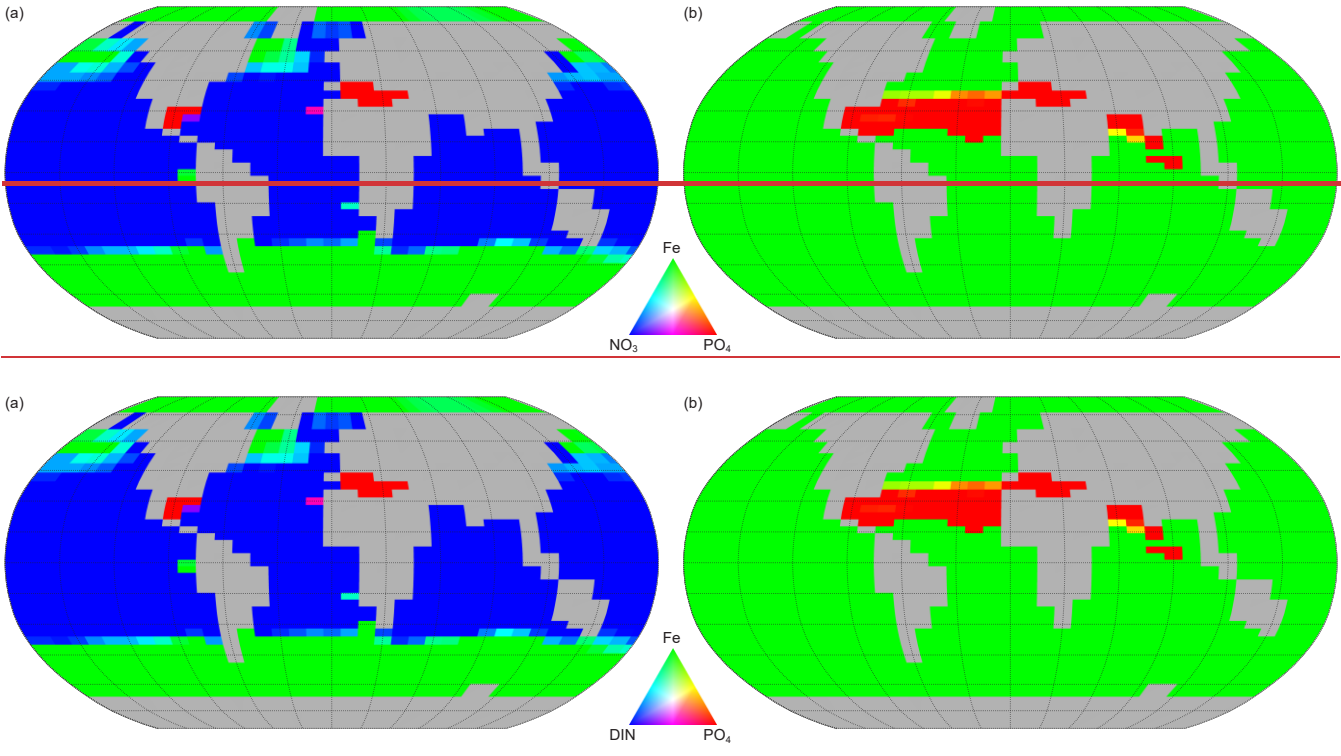

905 **Figure 15 Spatial variation of the limiting factor for nutrient uptake** (a-proxy for phytoplankton growth in NutGEnIE). For (a) other phytoplankton, red = PO4 limitation, green = Fe limitation, blue = DIN limitation. and (b) diazotrophs (will-are not be limited by NO₃NO_3 as nitrogen is considered freely available via nitrogen fixation). rRed = $PO_4^-$$PO_4$ limitation, green = Fe limitation, blue = NO₃ limitation.

38

Figure 15Figure 15 shows the limiting nutrient in each surface cell, in addition, supplementary figures providing the calculated limiting value for each nutrient are available in Fig. S46 to S49.

910

The additional diagnostic tools that have allowed the spatial variations in the limiting factors (Fig. 14) and PLN (Fig. 15) to be visualised are also reassuring. Given the proposed use of this configuration of NutGEnIE to investigate long term nutrient limitation of PP it is important that the spatial variations are realistic. Mahowald et al. (2017) (see Fig. 3 therein) produced schematic distributions of factor and nutrient limitation for differing phytoplankton classes. The results of NutGEnIE compare

915 well to the schematics of Mahowald et al. (2017). In addition, Browning and Moore (2023) (see Fig. 1 therein) carried out a global analysis of phytoplankton nutrient limitation, summarising over 100 bioassay experiments identifying the PLN. NutGEnIE (Fig. 15a) is aligned well with the summary of Browning and Moore (2023) although, two discrepancies are noteworthy. Firstly, NutGEnIE identifies phosphorus as the PLN in the Mediterranean Sea and a small area of the Caribbean, whereas in these areas Browning and Moore (2023) identify fixed nitrogen as the PLN with co- or serial phosphorus limitation.

920 Secondly, in NutGEnIE the area of the equatorial Pacific Ocean where iron is identified as the PLN is somewhat smaller than that identified by Browning and Moore (2023).

43.44.3 The ULN and future work

The flexibility NutGEnIE model allows for different continental configurations alongside varying atmospheric conditions that

925 would allow investigations of the impact of nutrient supply on PP in paleo-worlds scenarios (e.g. Wilson et al., 2018). NutGEnIE would also facilitate experiments or simulations that consider differing nutrient input fluxes and or residence times or differing nutrient requirements of phytoplankton.

Earlier we considered the distinction between the PLN and the ULN for oceanic PP. The limitations of previous work to identify the ULN have also been discussed along with required characteristic of any model intended to investigate the ULN

930 (Sect. 1.3). Aspects relating to the biogeochemical cycles of NutGEnIE and the ability to represent reality are summarised above. However, two additional critical aspects when investigating the ULN were detailed in Sect 1.3, the importance of an open system model and for model run times to considerably exceed the residence times of all nutrients. The open nutrient cycles have been detailed in Sect. 2.3 and NutGEnIE model runs in excess ofup to ~5100 kyr are feasible. NutGEnIE run compute times indicate are simulations approximately 10 000 simulation years per dayof 100 kyr would complete within a

935 two week duration. Phytoplankton stoichiometric requirements used in NutGEnIE are set via parameters, Table 2. These stoichiometric requirements are known to vary (e.g. King et al., 2012), the values of the associated parameters should be considered and potentially the subject of sensitivity analysis during the ULN investigations.

Comparisons between NutGEnIE and real ocean data (encompassing physical processes, nutrients, and BGC processes) have

940 been made and in each case the comparisons indicate that as configured here NutGEnIE is a suitable tool for the study of the ULN question. The proposed use here is to consider the limiting influences that nutrients have on ocean PP over the long term, therefore realistic surface nutrient concentrations are vital. Surface nutrient concentrations are influenced by both physical and BGC processes, hence the relevance in reviewing those aspects. The NutGEnIE model as configured here is representing Earth's oceans (area of ~361 x 10^{12} m^2, volume of ~135 x 10^{16} m^3) by a 36 x 36 grid with 16 depth levels. This level of

945 abstraction will not be able to accurately reproduce the complexities of ocean processes; it is however important that the most relevant processes are included with sufficient detail. Therefore, we have focused on whether a good representation rather than a perfect replication of the oceans has been obtained.

The CLIMBER-X model has several similarities to NutGEnIE (Willeit et al., 2023) and could also, if modified, be used to investigate the ULN for oceanic PP. CLIMBER-X has a higher resolution (5° x 5°) than NutGEnIE with 23 depth levels as

950 opposed to the 16 of NutGEnIE (Willeit et al., 2022). CLIMBER-X represents phytoplankton and zooplankton as tracers (Willeit et al., 2023) as opposed to the nutrient uptake approach of NutGEnIE. However, diazotrophs are disabled by default in CLIMBER-X and N_2 fixation is represented by a diagnostic formulation (Willeit et al., 2023). CLIMBER-X also has a closed phosphorus budget and the iron ligand association constant is fixed across the water column (Willeit et al., 2023). It would be interesting to compare results from the two models if CLIMBER-X were to be given explicit diazotrophs, open

955 nutrient cycles and depth-variable ligand behaviour. We suggest that the novel aspects of NutGEnIE (in particular the concurrent use of three open nutrient cycles and the dynamic ligand binding mechanism with stronger binding in the upper water column) presented here make it an appropriate option for investigating the ULN.(Willeit et al., 2023; Willeit et al., 2022)

455 Conclusions

960 Our motivation has been to create a model, NutGEnIE, that can be used to investigate the ULN for oceanic PP focusing onr the nitrogen, phosphorus and iron cycles. A key development has been to ensure that the modelled iron cycle is realistic by including a dynamic ligand mechanism. The novel aspect that each nutrient cycle is open with the ability for inventories to vary over time is of particular importance in the investigation of the ULN. The introduced surface fluxes of PO_4^- and NO_3^-, seafloor flux of Fe and existing dust supply of Fe provide mechanisms that will allow fertilisation simulations to investigate

965 the ULN

We have conducted an extensive validation of biogeochemical aspects of NutGEnIE by comparing pertinent tracers to real ocean observations in both surface waters and the ocean interior. This review has highlighted areas of discrepancies but, more importantly, supports the fact that, overall, NutGEnIE reflects the processes and state of the ocean with a high good degree of accuracy. Statistical comparisons of NutGEnIE properties to ocean observation have provided strong evidence that this

970 configuration of NutGEnIE is suitable to conduct the planned nutrient limitation analysis. We believe these validations support the suggestion that NutGEnIE can be used for that purpose and to investigate other questions related to the role of nutrients on oceanic biogeochemical processes.

The primary motivation behind establishing this configuration is to analyse the long-term influence of nutrient limitation on oceanic PP and we conclude that NutGEnIE, as configured and evaluated here, can support such a study. This configuration

975 of NutGEnIE can also be useful in the analysis of the dynamics of nutrient supply and oceanic PP in past, present or future scenarios.

Code availability

Data availability

Author contribution

DS developed the model and conducted the analysis with input from all authors. All authors wrote the manuscript.

Competing interests

Some authors are members of the editorial board of journal Geoscientific Model Development. The peer-review process was guided by an independent editor, and the authors have no other competing interests to declare.

Disclaimer

References

Archer, D. E. and Johnson, K.: A model of the iron cycle in the ocean, Global Biogeochemical Cycles, 14, 269-279, https://doi.org/10.1029/1999GB900053, 2000.
Ballantyne, A. P., Alden, C. B., Miller, J. B., Tans, P. P., and White, J.: Increase in observed net carbon dioxide uptake by land and oceans during the past 50 years, Nature, 488, 70-72, 2012.
Behrenfeld, M. J. and Falkowski, P. G.: Photosynthetic rates derived from satellite-based chlorophyll concentration, Limnology and Oceanography, 42, 1-20, https://doi.org/10.4319/lo.1997.42.1.0001, 1997.

Benitez-Nelson, C. R.: The biogeochemical cycling of phosphorus in marine systems, Earth-Science Reviews, 51, 109-135, https://doi.org/10.1016/S0012-8252(00)00018-0, 2000.

Berman-Frank, I., Quigg, A., Finkel, Z. V., Irwin, A. J., and Haramaty, L.: Nitrogen-fixation strategies and Fe requirements in cyanobacteria, Limnology and Oceanography, 52, 2260-2269, https://doi.org/10.4319/lo.2007.52.5.2260, 2007.

Bestion, E., Schaum, C.-E., and Yvon-Durocher, G.: Nutrient limitation constrains thermal tolerance in freshwater phytoplankton, Limnology and Oceanography Letters, 3, 436-443, https://doi.org/10.1002/lol2.10096, 2018.

Bissinger, J. E., Montagnes, D. J. S., harples, J., and Atkinson, D.: Predicting marine phytoplankton maximum growth rates from temperature: Improving on the Eppley curve using quantile regression, Limnology and Oceanography, 53, 487-493, https://doi.org/10.4319/lo.2008.53.2.0487, 2008.

Bonnet, S., Guieu, C., Bruyant, F., Prášil, O., Van Wambeke, F., Raimbault, P., Moutin, T., Grob, C., Gorbunov, M. Y., Zehr, J. P., Masquelier, S. M., Garczarek, L., and Claustre, H.: Nutrient limitation of primary productivity in the Southeast Pacific (BIOSOPE cruise), Biogeosciences, 5, 215-225, https://doi.org/10.5194/bg-5-215-2008, 2008.

Boyd, P. W. and Abraham, E. R.: Iron-mediated changes in phytoplankton photosynthetic competence during SOIREE, Deep Sea Research Part II: Topical Studies in Oceanography, 48, 2529-2550, https://doi.org/10.1016/S0967-0645(01)00007-8, 2001.

Boyd, P. W. and Tagliabue, A.: Using the L* concept to explore controls on the relationship between paired ligand and dissolved iron concentrations in the ocean, Marine Chemistry, 173, 52-66, https://doi.org/10.1016/j.marchem.2014.12.003, 2015.

Boyd, P. W., Claustre, H., Levy, M., Siegel, D. A., and Weber, T.: Multi-faceted particle pumps drive carbon sequestration in the ocean, Nature, 568, 327-335, https://doi.org/10.1038/s41586-019-1098-2, 2019.

Browning, T. J. and Moore, C. M.: Global analysis of ocean phytoplankton nutrient limitation reveals high prevalence of co-limitation, Nature Communications, 14, 5014, https://doi.org/10.1038/s41467-023-40774-0, 2023.

Cao, L., Eby, M., Ridgwell, A., Caldeira, K., Archer, D., Ishida, A., Joos, F., Matsumoto, K., Mikolajewicz, U., Mouchet, A., Orr, J. C., Plattner, G. K., Schlitzer, R., Tokos, K., Totterdell, I., Tschumi, T., Yamanaka, Y., and Yool, A.: The role of ocean transport in the uptake of anthropogenic CO_2, Biogeosciences, 6, 375-390, https://doi.org/10.5194/bg-6-375-2009, 2009.

Carr, M.-E., Friedrichs, M. A. M., Schmeltz, M., Noguchi Aita, M., Antoine, D., Arrigo, K. R., Asanuma, I., Aumont, O., Barber, R., Behrenfeld, M., Bidigare, R., Buitenhuis, E. T., Campbell, J., Ciotti, A., Dierssen, H., Dowell, M., Dunne, J., Esaias, W., Gentili, B., Gregg, W., Groom, S., Hoepffner, N., Ishizaka, J., Kameda, T., Le Quéré, C., Lohrenz, S., Marra, J., Mélin, F., Moore, K., Morel, A., Reddy, T. E., Ryan, J., Scardi, M., Smyth, T., Turpie, K., Tilstone, G., Waters, K., and Yamanaka, Y.: A comparison of global estimates of marine primary production from ocean color, Deep Sea Research Part II: Topical Studies in Oceanography, 53, 741-770, https://doi.org/10.1016/j.dsr2.2006.01.028, 2006.

Chisholm, S. W.: Stirring times in the Southern Ocean, Nature, 407, 685-686, https://doi.org/10.1038/35037696, 2000.

Codispoti, L. A., Brandes, J., Christensen, J. P., Devol, A. H., Naqvi, S. W. A., Paerl, H., and Yoshinari, T.: The oceanic fixed nitrogen and nitrous oxide budgets: moving targets as we enter the anthropocene?, Scientia Marina, 65, 85-105, 2001.

Cullen, J. J.: Hypotheses to explain high-nutrient conditions in the open sea, Limnology and Oceanography, 36, 1578-1599, https://doi.org/10.4319/lo.1991.36.8.1578, 1991.

de Baar, H. J. W.: von Liebig's law of the minimum and plankton ecology (1899–1991), Progress in Oceanography, 33, 347-386, https://doi.org/10.1016/0079-6611(94)90022-1, 1994.

Delaney, M. L.: Phosphorus accumulation in marine sediments and the oceanic phosphorus cycle, Global Biogeochemical Cycles, 12, 563-572, https://doi.org/10.1029/98GB02263, 1998.

Deutsch, C., Sarmiento, J. L., Sigman, D. M., Gruber, N., and Dunne, J. P.: Spatial coupling of nitrogen inputs and losses in the ocean, Nature, 445, 163-167, https://doi.org/10.1038/nature05392, 2007.

Doney, S. C., Lindsay, K., Fung, I., and John, J.: Natural Variability in a Stable, 1000-Yr Global Coupled Climate–Carbon Cycle Simulation, Journal of Climate, 19, 3033-3054, https://doi.org/10.1175/jcli3783.1, 2006.

Edwards, N. R. and Marsh, R.: Uncertainties due to transport-parameter sensitivity in an efficient 3-D ocean-climate model, Climate Dynamics, 24, 415-433, https://doi.org/10.1007/s00382-004-0508-8, 2005.

Eppley, R. W.: Temperature and phytoplankton growth in the sea, Fish. bull, 70, 1063-1085, 1972.

Falkowski, P. G.: Evolution of the nitrogen cycle and its influence on the biological sequestration of $CO2$ in the ocean, Nature, 387, 272-275, 1997.

Flynn, K. J.: Ecological modelling in a sea of variable stoichiometry: dysfunctionality and the legacy of Redfield and Monod, Progress in Oceanography, 84, 52-65, 2010.

Friedlingstein, P., Jones, M. W., O'Sullivan, M., Andrew, R. M., Bakker, D. C. E., Hauck, J., Le Quéré, C., Peters, G. P., Peters, W., Pongratz, J., Sitch, S., Canadell, J. G., Ciais, P., Jackson, R. B., Alin, S. R., Anthoni, P., Bates, N. R., Becker, M., Bellouin, N., Bopp, L., Chau, T. T. T., Chevallier, F., Chini, L. P., Cronin, M., Currie, K. I., Decharme, B., Djeutchouang, L. M., Dou, X., Evans, W., Feely, R. A., Feng, L., Gasser, T., Gilfillan, D., Gkritzalis, T., Grassi, G., Gregor, L., Gruber, N., Gürses, Ö., Harris, I., Houghton, R. A., Hurtt, G. C., Iida, Y., Ilyina, T., Luijkx, I. T., Jain, A., Jones, S. D., Kato, E., Kennedy, D., Klein Goldewijk, K., Knauer, J., Korsbakken, J. I., Körtzinger, A., Landschützer, P., Lauvset, S. K., Lefèvre, N., Lienert, S., Liu, J., Marland, G., McGuire, P. C., Melton, J. R., Munro, D. R., Nabel, J. E. M. S., Nakaoka, S. I., Niwa, Y., Ono, T., Pierrot, D., Poulter, B., Rehder, G., Resplandy, L., Robertson, E., Rödenbeck, C., Rosan, T. M., Schwinger, J., Schwingshackl, C., Séférian, R., Sutton, A. J., Sweeney, C., Tanhua, T., Tans, P. P., Tian, H., Tilbrook, B., Tubiello, F., van der Werf, G. R., Vuichard, N., Wada, C., Wanninkhof, R., Watson, A. J., Willis, D., Wiltshire, A. J., Yuan, W., Yue, C., Yue, X., Zaehle, S., and Zeng, J.: Global Carbon Budget 2021, Earth Syst. Sci. Data, 14, 1917-2005, 10.5194/essd-14-1917-2022, 2022.

Froelich, P. N., Klinkhammer, G. P., Bender, M. L., Luedtke, N. A., Heath, G. R., Cullen, D., Dauphin, P., Hammond, D., Hartman, B., and Maynard, V.: Early oxidation of organic matter in pelagic sediments of the eastern equatorial Atlantic: suboxic diagenesis, Geochimica et Cosmochimica Acta, 43, 1075-1090, https://doi.org/10.1016/0016-7037(79)90095-4, 1979.

Fung, I. Y., Meyn, S. K., Tegen, I., Doney, S. C., John, J. G., and Bishop, J. K. B.: Iron supply and demand in the upper ocean, Global Biogeochemical Cycles, 14, 281-295, https://doi.org/10.1029/1999GB900059, 2000.

Galbraith, E. D. and Skinner, L. C.: The Biological Pump During the Last Glacial Maximum, Annual Review of Marine Science, 12, 559-586, https://doi.org/10.1146/annurev-marine-010419-010906, 2020.

Galloway, J. N., Dentener, F. J., Capone, D. G., Boyer, E. W., Howarth, R. W., Seitzinger, S. P., Asner, G. P., Cleveland, C. C., Green, P. A., Holland, E. A., Karl, D. M., Michaels, A. F., Porter, J. H., Townsend, A. R., and Vöosmarty, C. J.: Nitrogen Cycles: Past, Present, and Future, Biogeochemistry, 70, 153-226, https://doi.org/10.1007/s10533-004-0370-0, 2004.

Garcia, H., Weathers, K., Paver, C., Smolyar, I., Boyer, T., Locarnini, M., Zweng, M., Mishonov, A., Baranova, O., and Seidov, D.: World ocean atlas 2018. Volume 4, Dissolved inorganic nutrients (phosphate, nitrate and nitrate+nitrite, silicate), 2018a.

Garcia, H., Weathers, K., Paver, C., Smolyar, I., Boyer, T., Locarnini, M., Zweng, M., Mishonov, A., Baranova, O., and Seidov, D.: World ocean atlas 2018, Volume 3: Dissolved Oxygen, Apparent Oxygen Utilization, and Dissolved Oxygen Saturation, 2018b.

1085 GEOTRACES - An International Study of the Marine Biogeochemical Cycles of Trace Elements and Isotopes: https://www.geotraces.org/, last access: 1 June 2022.

GEOTRACES Intermediate Data Product Group: The GEOTRACES Intermediate Data Product 2021 (IDP2021), NERC EDS British Oceanographic Data Centre NOC, https://doi.org/doi:10.5285/cf2d9ba9-d51d-3b7c-e053-8486abc0f5fd, 2021.

Gillooly, J. F., Charnov, E. L., West, G. B., Savage, V. M., and Brown, J. H.: Effects of size and temperature on developmental time, Nature, 1090 417, 70-73, https://doi.org/10.1038/417070a, 2002.

Grimaud, G. M., Mairet, F., Sciandra, A., and Bernard, O.: Modeling the temperature effect on the specific growth rate of phytoplankton: a review, Reviews in Environmental Science and Bio/Technology, 16, 625-645, 2017.

Gruber, N.: The dynamics of the marine nitrogen cycle and atmospheric CO2. In ''Carbon Climate interactions''(Oguz, T., and Follows, M., eds.), 2004.

1095 Gruber, N.: Chapter 1 - The Marine Nitrogen Cycle: Overview and Challenges, in: Nitrogen in the Marine Environment (Second Edition), edited by: Capone, D. G., Bronk, D. A., Mulholland, M. R., and Carpenter, E. J., Academic Press, San Diego, 1-50, https://doi.org/10.1016/B978-0-12-372522-6.00001-3, 2008.

Gruber, N. and Sarmiento, J. L.: Global patterns of marine nitrogen fixation and denitrification, Global Biogeochemical Cycles, 11, 235-266, https://doi.org/10.1029/97GB00077, 1997.

1100 Hain, M., Sigal, D., and Haug, G.: The biological pump in the past. Reference module in earth systems and environmental sciences, treatise on geochemistry (2nd edn). The oceans and marine geochemistry, 2014.

Hayes, C. T., Anderson, R. F., Cheng, H., Conway, T. M., Edwards, R. L., Fleisher, M. Q., Ho, P., Huang, K.-F., John, S. G., Landing, W. M., Little, S. H., Lu, Y., Morton, P. L., Moran, S. B., Robinson, L. F., Shelley, R. U., Shiller, A. M., and Zheng, X.-Y.: Replacement Times of a Spectrum of Elements in the North Atlantic Based on Thorium Supply, Global Biogeochemical Cycles, 32, 1294-1311, 1105 https://doi.org/10.1029/2017GB005839, 2018.

Hoffmann, L. J., Peeken, I., Lochte, K., Assmy, P., and Veldhuis, M.: Different reactions of Southern Ocean phytoplankton size classes to iron fertilization, Limnology and Oceanography, 51, 1217-1229, https://doi.org/10.4319/lo.2006.51.3.1217, 2006.

Honeyman, B. D., Balistrieri, L. S., and Murray, J. W.: Oceanic trace metal scavenging: the importance of particle concentration, Deep Sea Research Part A. Oceanographic Research Papers, 35, 227-246, https://doi.org/10.1016/0198-0149(88)90038-6, 1988.

1110 Hunter, K. A. and Boyd, P. W.: Iron-binding ligands and their role in the ocean biogeochemistry of iron, Environmental Chemistry, 4, 221-232, https://doi.org/10.1071/EN07012, 2007.

Johnson, K. S. and Bif, M. B.: Constraint on net primary productivity of the global ocean by Argo oxygen measurements, Nature Geoscience, 14, 769-774, https://doi.org/10.1038/s41561-021-00807-z, 2021.

King, A. L., Sañudo-Wilhelmy, S. A., Boyd, P. W., Twining, B. S., Wilhelm, S. W., Breene, C., Ellwood, M. J., and Hutchins, D. A.: A 1115 comparison of biogenic iron quotas during a diatom spring bloom using multiple approaches, Biogeosciences, 9, 667-687, https://doi.org/10.5194/bg-9-667-2012, 2012.

Lam, P., Lavik, G., Jensen, M. M., van de Vossenberg, J., Schmid, M., Woebken, D., Gutiérrez, D., Amann, R., Jetten, M. S. M., and Kuypers, M. M. M.: Revising the nitrogen cycle in the Peruvian oxygen minimum zone, Proceedings of the National Academy of Sciences, 106, 4752-4757, https://doi.org/10.1073/pnas.0812444106, 2009.

1120 Lenton, T. M. and Watson, A. J.: Redfield revisited: 1. Regulation of nitrate, phosphate, and oxygen in the ocean, Global Biogeochemical Cycles, 14, 225-248, https://doi.org/10.1029/1999GB900065, 2000.

Locarnini, M., Mishonov, A., Baranova, O., Boyer, T., Zweng, M., Garcia, H., Seidov, D., Weathers, K., Paver, C., and Smolyar, I.: World ocean atlas 2018, volume 1: Temperature, 2018.

Luo, C., Mahowald, N. M., Meskhidze, N., Chen, Y., Siefert, R. L., Baker, A. R., and Johansen, A. M.: Estimation of iron solubility from 1125 observations and a global aerosol model, Journal of Geophysical Research: Atmospheres, 110, https://doi.org/10.1029/2005JD006059, 2005.

Luo, Y. W., Doney, S. C., Anderson, L. A., Benavides, M., Berman-Frank, I., Bode, A., Bonnet, S., Boström, K. H., Böttjer, D., Capone, D. G., Carpenter, E. J., Chen, Y. L., Church, M. J., Dore, J. E., Falcón, L. I., Fernández, A., Foster, R. A., Furuya, K., Gómez, F., Gundersen, K., Hynes, A. M., Karl, D. M., Kitajima, S., Langlois, R. J., LaRoche, J., Letelier, R. M., Marañón, E., McGillicuddy Jr, D. J., Moisander, P. H., Moore, C. M., Mouriño-Carballido, B., Mulholland, M. R., Needoba, J. A., Orcutt, K. M., Poulton, A. J., Rahav, E., Raimbault, P., 1130 Rees, A. P., Riemann, L., Shiozaki, T., Subramaniam, A., Tyrrell, T., Turk-Kubo, K. A., Varela, M., Villareal, T. A., Webb, E. A., White, A. E., Wu, J., and Zehr, J. P.: Database of diazotrophs in global ocean: abundance, biomass and nitrogen fixation rates, Earth Syst. Sci. Data, 4, 47-73, https://doi.org/10.5194/essd-4-47-2012, 2012.

Mahowald, N. M., Muhs, D. R., Levis, S., Rasch, P. J., Yoshioka, M., Zender, C. S., and Luo, C.: Change in atmospheric mineral aerosols in response to climate: Last glacial period, preindustrial, modern, and doubled carbon dioxide climates, Journal of Geophysical Research: 1135 Atmospheres, 111, https://doi.org/10.1029/2005JD006653, 2006.

Mahowald, N. M., Scanza, R., Brahney, J., Goodale, C. L., Hess, P. G., Moore, J. K., and Neff, J.: Aerosol Deposition Impacts on Land and Ocean Carbon Cycles, Current Climate Change Reports, 3, 16-31, https://doi.org/10.1007/s40641-017-0056-z, 2017.

Maier-Reimer, E.: Geochemical cycles in an ocean general circulation model. Preindustrial tracer distributions, Global Biogeochemical Cycles, 7, 645-677, https://doi.org/10.1029/93GB01355, 1993.

1140 Marra, J., Heinemann, K., and Landriau, G.: Observed and predicted measurements of photosynthesis in a phytoplankton culture exposed to natural irradiance, Marine Ecology-progress Series - MAR ECOL-PROGR SER, 24, 43-50, https://doi.org/10.3354/meps024043, 1985.

Marsh, R., Müller, S. A., Yool, A., and Edwards, N. R.: Incorporation of the C-GOLDSTEIN efficient climate model into the GENIE framework: "eb_go_gs" configurations of GENIE, Geosci. Model Dev., 4, 957-992, https://doi.org/10.5194/gmd-4-957-2011, 2011.

Martin, J. H.: Glacial-interglacial CO2 change: The Iron Hypothesis, Paleoceanography, 5, 1-13, https://doi.org/10.1029/PA005i001p00001, 1145 1990.

Martin, J. H., Coale, K. H., Johnson, K. S., Fitzwater, S. E., Gordon, R. M., Tanner, S. J., Hunter, C. N., Elrod, V. A., Nowicki, J. L., Coley, T. L., Barber, R. T., Lindley, S., Watson, A. J., Van Scoy, K., Law, C. S., Liddicoat, M. I., Ling, R., Stanton, T., Stockel, J., Collins, C., Anderson, A., Bidigare, R., Ondrusek, M., Latasa, M., Millero, F. J., Lee, K., Yao, W., Zhang, J. Z., Friederich, G., Sakamoto, C., Chavez, F., Buck, K., Kolber, Z., Greene, R., Falkowski, P., Chisholm, S. W., Hoge, F., Swift, R., Yungel, J., Turner, S., Nightingale, P., Hatton, A., 1150 Liss, P., and Tindale, N. W.: Testing the iron hypothesis in ecosystems of the equatorial Pacific Ocean, Nature, 371, 123-129, https://doi.org/10.1038/371123a0, 1994.

Mills, M. M., Ridame, C., Davey, M., La Roche, J., and Geider, R. J.: Iron and phosphorus co-limit nitrogen fixation in the eastern tropical North Atlantic, Nature, 429, 292-294, https://doi.org/10.1038/nature02550, 2004.

Misumi, K., Lindsay, K., Moore, J. K., Doney, S. C., Tsumune, D., and Yoshida, Y.: Humic substances may control dissolved iron distributions in the global ocean: Implications from numerical simulations, Global Biogeochemical Cycles, 27, 450-462, https://doi.org/10.1002/gbc.20039, 2013.

Monteiro, F. M., Dutkiewicz, S., and Follows, M. J.: Biogeographical controls on the marine nitrogen fixers, Global Biogeochemical Cycles, 25, https://doi.org/10.1029/2010GB003902, 2011.

Monteiro, F. M., Pancost, R. D., Ridgwell, A., and Donnadieu, Y.: Nutrients as the dominant control on the spread of anoxia and euxinia across the Cenomanian-Turonian oceanic anoxic event (OAE2): Model-data comparison, Paleoceanography, 27, https://doi.org/10.1029/2012PA002351, 2012.

Moore, C. M.: Diagnosing oceanic nutrient deficiency, Philosophical Transactions of the Royal Society A: Mathematical, Physical and Engineering Sciences, 374, 20150290, https://doi.org/doi:10.1098/rsta.2015.0290, 2016.

Moore, C. M., Mills, M. M., Langlois, R., Milne, A., Achterberg, E. P., La Roche, J., and Geider, R. J.: Relative influence of nitrogen and phosphorous availability on phytoplankton physiology and productivity in the oligotrophic sub-tropical North Atlantic Ocean, Limnology and Oceanography, 53, 291-305, https://doi.org/10.4319/lo.2008.53.1.0291, 2008.

Moore, C. M., Mills, M. M., Arrigo, K. R., Berman-Frank, I., Bopp, L., Boyd, P. W., Galbraith, E. D., Geider, R. J., Guieu, C., Jaccard, S. L., Jickells, T. D., La Roche, J., Lenton, T. M., Mahowald, N. M., Marañón, E., Marinov, I., Moore, J. K., Nakatsuka, T., Oschlies, A., Saito, M. A., Thingstad, T. F., Tsuda, A., and Ulloa, O.: Processes and patterns of oceanic nutrient limitation, Nature Geoscience, 6, 701-710, https://doi.org/10.1038/ngeo1765, 2013.

Moore, J. K. and Braucher, O.: Sedimentary and mineral dust sources of dissolved iron to the world ocean, Biogeosciences, 5, 631-656, https://doi.org/10.5194/bg-5-631-2008, 2008.

Moore, J. K. and Doney, S. C.: Iron availability limits the ocean nitrogen inventory stabilizing feedbacks between marine denitrification and nitrogen fixation, Global Biogeochemical Cycles, 21, https://doi.org/10.1029/2006GB002762, 2007.

Naafs, B. D. A., Monteiro, F. M., Pearson, A., Higgins, M. B., Pancost, R. D., and Ridgwell, A.: Fundamentally different global marine nitrogen cycling in response to severe ocean deoxygenation, Proceedings of the National Academy of Sciences, 116, 24979-24984, https://doi.org/10.1073/pnas.1905553116, 2019.

Najjar, R. and Orr, J.: Biotic-HOWTO. Internal OCMIP Report, LSCE/CEA Saclay, Gif-sur-Yvette, France, 15 pp, 1999.

O'Donnell, D. R., Hamman, C. R., Johnson, E. C., Kremer, C. T., Klausmeier, C. A., and Litchman, E.: Rapid thermal adaptation in a marine diatom reveals constraints and trade-offs, Global change biology, 24, 4554-4565, 2018.

Ocean Productivity: http://orca.science.oregonstate.edu/index.php, last access: 1 June 2024.

Olson, S. L., Reinhard, C. T., and Lyons, T. W.: Limited role for methane in the mid-Proterozoic greenhouse, Proceedings of the National Academy of Sciences, 113, 11447-11452, https://doi.org/doi:10.1073/pnas.1608549113, 2016.

Parekh, P., Follows, M. J., and Boyle, E.: Modeling the global ocean iron cycle, Global Biogeochemical Cycles, 18, https://doi.org/10.1029/2003GB002061, 2004.

Parekh, P., Follows, M. J., and Boyle, E. A.: Decoupling of iron and phosphate in the global ocean, Global Biogeochemical Cycles, 19, https://doi.org/10.1029/2004GB002280, 2005.

Redfield, A. C.: On the proportions of organic derivatives in sea water and their relation to the composition of plankton, University Press of Liverpool Liverpool1934.

Redfield, A. C.: THE BIOLOGICAL CONTROL OF CHEMICAL FACTORS IN THE ENVIRONMENT, American Scientist, 46, 230A-221, 1958.

Reinhard, C. T., Olson, S. L., Kirtland Turner, S., Pälike, C., Kanzaki, Y., and Ridgwell, A.: Oceanic and atmospheric methane cycling in the cGENIE Earth system model – release v0.9.14, Geosci. Model Dev., 13, 5687-5706, https://doi.org/10.5194/gmd-13-5687-2020, 2020.

Ridgwell, A., Hargreaves, J. C., Edwards, N. R., Annan, J. D., Lenton, T. M., Marsh, R., Yool, A., and Watson, A.: Marine geochemical data assimilation in an efficient Earth System Model of global biogeochemical cycling, Biogeosciences, 4, 87-104, https://doi.org/10.5194/bg-4-87-2007, 2007.

Sarmiento, J. L., Hughes, T. M. C., Stouffer, R. J., and Manabe, S.: Simulated response of the ocean carbon cycle to anthropogenic climate warming, Nature, 393, 245-249, https://doi.org/10.1038/30455, 1998.

Schlesinger, W. H.: 9 - The Sea, in: Biogeochemistry: an Analysis of Global Change, edited by: Schlesinger, W. H., Academic Press, 254-293, https://doi.org/10.1016/B978-0-12-625157-9.50014-9, 1991.

Sigman, D. M. and Hain, M. P.: The biological productivity of the ocean, Nature Education Knowledge, 3, 1-16, 2012.

Silsbe, G. M., Behrenfeld, M. J., Halsey, K. H., Milligan, A. J., and Westberry, T. K.: The CAFE model: A net production model for global ocean phytoplankton, Global Biogeochemical Cycles, 30, 1756-1777, https://doi.org/10.1002/2016GB005521, 2016.

Sohm, J. A., Webb, E. A., and Capone, D. G.: Emerging patterns of marine nitrogen fixation, Nature Reviews Microbiology, 9, 499-508, https://doi.org/10.1038/nrmicro2594, 2011.

Sommer, U.: Nitrate- and silicate-competition among antarctic phytoplankton, Marine Biology, 91, 345-351, https://doi.org/10.1007/BF00428628, 1986.

Stappard, D.: Code and data for "NutGEnIE 1.0: nutrient cycle extensions to the cGEnIE Earth system model to examine the long-term influence of nutrients on oceanic primary production". Zenodo, https://doi.org/10.5281/zenodo.16754587, 2025.

Stappard, D. A., Wilson, J. D., Yool, A., and Tyrrell, T.: NutGEnIE 1.0: nutrient cycle extensions to the cGEnIE Earth system model to examine the long-term influence of nutrients on oceanic primary production, EGUsphere, 2025, 1-33, https://doi.org/10.5194/egusphere-2025-436, 2025.

Tagliabue, A., Bowie, A. R., Boyd, P. W., Buck, K. N., Johnson, K. S., and Saito, M. A.: The integral role of iron in ocean biogeochemistry, Nature, 543, 51-59, https://doi.org/10.1038/nature21058, 2017.

Tagliabue, A., Bopp, L., Dutay, J.-C., Bowie, A. R., Chever, F., Jean-Baptiste, P., Bucciarelli, E., Lannuzel, D., Remenyi, T., Sarthou, G., Aumont, O., Gehlen, M., and Jeandel, C.: Hydrothermal contribution to the oceanic dissolved iron inventory, Nature Geoscience, 3, 252-256, https://doi.org/10.1038/ngeo818, 2010.

Tagliabue, A., Aumont, O., DeAth, R., Dunne, J. P., Dutkiewicz, S., Galbraith, E., Misumi, K., Moore, J. K., Ridgwell, A., Sherman, E., Stock, C., Vichi, M., Völker, C., and Yool, A.: How well do global ocean biogeochemistry models simulate dissolved iron distributions?, Global Biogeochemical Cycles, 30, 149-174, https://doi.org/10.1002/2015GB005289, 2016.

Taylor, K. E.: Summarizing multiple aspects of model performance in a single diagram, Journal of Geophysical Research: Atmospheres, 106, 7183-7192, https://doi.org/10.1029/2000JD900719, 2001.

Timmermans, K. R., van der Wagt, B., and de Baar, H. J. W.: Growth rates, half-saturation constants, and silicate, nitrate, and phosphate depletion in relation to iron availability of four large, open-ocean diatoms from the Southern Ocean, Limnology and Oceanography, 49, 2141-2151, https://doi.org/10.4319/lo.2004.49.6.2141, 2004.

Tyrrell, T.: The relative influences of nitrogen and phosphorus on oceanic primary production, Nature, 400, 525-531, https://doi.org/10.1038/22941, 1999.

van de Velde, S. J., Hülse, D., Reinhard, C. T., and Ridgwell, A.: Iron and sulfur cycling in the cGENIE.muffin Earth system model (v0.9.21), Geosci. Model Dev., 14, 2713-2745, https://doi.org/10.5194/gmd-14-2713-2021, 2021.

1230 Völker, C. and Tagliabue, A.: Modeling organic iron-binding ligands in a three-dimensional biogeochemical ocean model, Marine Chemistry, 173, 67-77, https://doi.org/10.1016/j.marchem.2014.11.008, 2015.

Wang, W.-L., Moore, J. K., Martiny, A. C., and Primeau, F. W.: Convergent estimates of marine nitrogen fixation, Nature, 566, 205-211, https://doi.org/10.1038/s41586-019-0911-2, 2019.

Westberry, T., Behrenfeld, M. J., Siegel, D. A., and Boss, E.: Carbon-based primary productivity modeling with vertically resolved 1235 photoacclimation, Global Biogeochemical Cycles, 22, https://doi.org/10.1029/2007GB003078, 2008.

Willeit, M., Ganopolski, A., Robinson, A., and Edwards, N. R.: The Earth system model CLIMBER-X v1.0 – Part 1: Climate model description and validation, Geosci. Model Dev., 15, 5905-5948, https://doi.org/10.5194/gmd-15-5905-2022, 2022.

Willeit, M., Ilyina, T., Liu, B., Heinze, C., Perrette, M., Heinemann, M., Dalmonech, D., Brovkin, V., Munhoven, G., Börker, J., Hartmann, J., Romero-Mujalli, G., and Ganopolski, A.: The Earth system model CLIMBER-X v1.0 – Part 2: The global carbon cycle, Geosci. Model 1240 Dev., 16, 3501-3534, https://doi.org/10.5194/gmd-16-3501-2023, 2023.

Wilson, J. D., Monteiro, F. M., Schmidt, D. N., Ward, B. A., and Ridgwell, A.: Linking Marine Plankton Ecosystems and Climate: A New Modeling Approach to the Warm Early Eocene Climate, Paleoceanography and Paleoclimatology, 33, 1439-1452, https://doi.org/10.1029/2018PA003374, 2018.

Witter, A. E., Hutchins, D. A., Butler, A., and Luther, G. W.: Determination of conditional stability constants and kinetic constants for strong 1245 model Fe-binding ligands in seawater, Marine Chemistry, 69, 1-17, https://doi.org/10.1016/S0304-4203(99)00087-0, 2000.

Yang, X., Liu, L., Yin, Z., Wang, X., Wang, S., and Ye, Z.: Quantifying photosynthetic performance of phytoplankton based on photosynthesis–irradiance response models, Environmental Sciences Europe, 32, 1-13, 2020.

Ye, Y., Völker, C., and Gledhill, M.: Exploring the Iron-Binding Potential of the Ocean Using a Combined pH and DOC Parameterization, Global Biogeochemical Cycles, 34, e2019GB006425, https://doi.org/10.1029/2019GB006425, 2020.

1250 Ye, Y., Völker, C., and Wolf-Gladrow, D. A.: A model of Fe speciation and biogeochemistry at the Tropical Eastern North Atlantic Time-Series Observatory site, Biogeosciences, 6, 2041-2061, https://doi.org/10.5194/bg-6-2041-2009, 2009.

Yool, A., Palmiéri, J., Jones, C. G., de Mora, L., Kuhlbrodt, T., Popova, E. E., Nurser, A. J. G., Hirschi, J., Blaker, A. T., Coward, A. C., Blockley, E. W., and Sellar, A. A.: Evaluating the physical and biogeochemical state of the global ocean component of UKESM1 in CMIP6 historical simulations, Geosci. Model Dev., 14, 3437-3472, https://doi.org/10.5194/gmd-14-3437-2021, 2021.

1255 Zehr, J. P. and Capone, D. G.: Changing perspectives in marine nitrogen fixation, Science, 368, eaay9514, https://doi.org/doi:10.1126/science.aay9514, 2020.

Zweng, M., Seidov, D., Boyer, T., Locarnini, M., Garcia, H., Mishonov, A., Baranova, O., Weathers, K., Paver, C., and Smolyar, I.: World ocean atlas 2018, volume 2: Salinity, 2018.